Agricultural and Forest Meteorology 362 (2025) 110341

Contents lists available at ScienceDirect

Agricultural and Forest Meteorology

journal homepage: www.elsevier.com/locate/agrformet

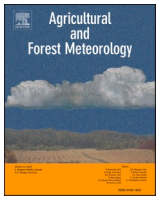

Unlocking the potential of Airborne LiDAR for direct assessment of fuel bulk density and load distributions for wildfire hazard mapping

Olivier Martin-Ducup [a,*], Jean-Luc Dupuy [a], Maxime Soma [b], Juan Guerra-Hernandez [c], Eva Marino [f,l], Paulo M. Fernandes [d,e], Ariadna Just [g], Jordi Corbera [g], Marion Toutchkov [h], Charlie Sorribas [a], Jerome Bock [i], Alexandre Piboule [j], Francesco Pirotti [k], François Pimont [a]

[a] Ecologie des Forêts Méditerranéennes (URFM), INRAE, F-84914 Avignon, France
[b] INRAE, Aix Marseille Univ, RECOVER, 13182, Aix-en-Provence, France
[c] Forest Research Centre (CEF), Associate Laboratory TERRA, School of Agriculture, University of Lisbon, Tapada da Ajuda, 1349-017 Lisboa, Portugal
[d] Centre for the Research and Technology of Agro-Environmental and Biological Sciences, CITAB, University of Trás-os-Montes and Alto Douro, Quinta dos Prados, 5000-801 Vila Real, Portugal
[e] ForestWISE—Collaborative Laboratory for Integrated Forest and Fire Management, Quinta de Prados, 5000-801 Vila Real, Portugal
[f] AGRESTA Sociedad.Cooperativa, c/Duque de Fernán Núñez 2, 28012 Madrid, Spain
[g] Cartographic and Geological Institute of Catalonia (ICGC), Parc de Montjuïc, Barcelona, Spain
[h] Mission Zonale DFCI, ONF, Aix en Provence, France
[i] Pôle Recherche, Développement et Innovation, Office National des Forêts, Site de Nancy-Brabois, 54600 Villers-lès-Nancy, France
[j] Pôle Recherche, Développement et Innovation, Office National des Forêts, 17 rue des diables bleus - CS 92628 Chambéry 73026, France
[k] TESAF Department, University of Padova, Viale dell'Università 16, Italy
[l] Instituto Nacional de Investigación y Tecnología Agraria y Alimentaria (INIA), Agencia Estatal Consejo Superior de Investigaciones Científicas (CSIC), Carretera de La Coruña 8, Madrid, 28040, Spain

ARTICLE INFO

Keywords:
Fuel metrics
Leaf area density
Clumping factor
Vegetation vertical profile
Fire behavior
Fuel mapping
Vegetation structure

ABSTRACT

Large-scale mapping of fuel load and fuel vertical distribution is essential for assessing fire danger, setting strategic goals and actions, and determining long-term resource needs. The Airborne LiDAR system can fulfil such goal by accurately capturing the three-dimensional arrangement of vegetation at regional and national scales.

We developed a novel method to estimate multiple metrics of fuel load and vertical bulk density distribution for any type of vegetation. The approach uses Beer-Lambert law for inverting the ALS point cloud into vertical plant area density profiles, which are converted into vertical bulk density distribution profiles using species-specific plant traits. The approach is evaluated by comparing ALS-based vegetation profiles and fuel metrics with field-based data from southeastern France, Spain, and Portugal for a range of vegetation types.

ALS-based and field-based vertical vegetation profiles were consistent. The range of values of fuel load metrics was also consistent with field data. Good correlations and low bias were attained for simple stratified structure with R^2 of 0.6, 0.42 and 0.68 and bias of -5 %, -2 % and -3.3 % for canopy base height, canopy fuel load, and canopy bulk density respectively. However, correlations were low for complex vertical structures. The use of species-specific plant traits appeared relevant by lowering the deviation between field and ALS-based values for most species.

Our field-independent fuel metric estimation shows comparable performance to results in the literature based on classification approaches trained on field metrics, highlighting the generality of our direct approach. We demonstrated how our approach is more relevant than field data for defining vertical vegetation strata in complex forest structures. We showed an application of the methods by mapping multiple metrics at regional scale (6343 km^2) such as canopy base height, fuel strata gap, and canopy and understory fuel loads. Our approach is adequate for feeding next generation models of wildfire risk assessment systems, enhanced by more flexible and accurate fuel data than the existing fuel typologies.

* Corresponding author.
E-mail address: olivier.martin.1@inrae.fr (O. Martin-Ducup).

https://doi.org/10.1016/j.agrformet.2024.110341
Received 18 April 2024; Received in revised form 14 November 2024; Accepted 25 November 2024
Available online 11 December 2024

1. Introduction

Fuel characteristics strongly affect wildfire behavior and activity (Keane, 2015). On the one hand, these characteristics relate to its water status or fuel moisture, which depends on the daily to monthly responses of living and dead elements of vegetation to weather. On the other hand, they relate to the quantity and spatial arrangement of the fuel elements, which varies on a longer time scale with vegetation structure and composition. While monitoring water status is important to assess daily danger and to implement early warning and preparedness, determining the structural characteristics of fuels is a major challenge for fire risk mapping, strategic planning, managing the ecological and socioeconomic consequences, and targeting forest and fire management policies (Arroyo et al., 2008; Fernandes, 2009).

Fire behavior theoretically depends on the three-dimensional distribution of bulk density (i.e. mass per unit volume, in kg m^{-3}) of fine fuel elements, conventionally thinner than 6 mm (Dupuy and Morvan, 2005). Generally speaking, the ability of the fire to spread in the surface, understory, and canopy layers of vegetation, is enhanced by increased horizontal and vertical fuel continuity (Reinhardt et al., 2006).

Because the fuel spatial distribution is highly challenging to measure in the field and to translate in terms of fire behavior, a long history of fire behavior modeling has identified several measurable fuel characteristics that simplify the complex three-dimensional arrangement of fuel and that are largely used for predicting key fire behavior metrics (Finney, 1998; Rothermel, 1972; Van Wagner, 1977). According to Byram's equation, the intensity of the fire is proportional to the load (mass per unit of ground area in kg m^{-2}) of fuels consumed in the flaming front and to the rate of spread of the fire (Byram, 1959). While surface fuels drive the initial spread of a forest fire, assessing the ability of fire to spread from the surface to the canopy is important because crown fires are the most intense and difficult to control (Werth et al., 2016). Crown fire initiation depends primarily on the intensity of the surface fire and on the fuel strata gap (FSG), while crown fire spread depends on the canopy bulk density (CBD) (Cruz et al., 2003, 2006). Canopy fuel load (CFL) allows to estimate mean CBD when the mean crown length is known, influences crown fire intensity directly, and often is estimated from the combination of forest inventory data and allometric equations. The FSG correspond to the distance between the top of the understory vegetation and the bottom of the overstorey canopy. . When understory vegetation is absent, the FSG is equal to the canopy base height (CBH), which has been defined as the height at which the bulk density is high enough to spread a fire (Reinhardt et al., 2006; Sando and Wick, 1972; Scott and Reinhardt, 2001). However, this definition raises the question of the exact threshold for the critical amount of fuel (Arkin et al., 2023; Scott and Reinhardt, 2001); and also its field measurement is subjective. A more practical definition of CBH on the field is the average height of the first live branches of main or dominant trees in a stand, which is often used in forestry surveys beyond wildfire studies (e.g. national forest inventories), as a general forest structure variable. According to the Van Wagner (1977) model for crown fire initiation, CBH has the greatest impact on crown fire occurrence. However, fire modelling systems that include Van Wagner (1977) model for crown fire initiation have several limitations under continuous-multilayered vertical fuel distribution and the model has not been calibrated for deciduous or mixed forests. Therefore, most model predictions of wildland fire behavior are inaccurate because the fuel complex is not uniform, continuous and homogeneous (Cruz and Alexander, 2013). To date, the consistency between the forestry definition of CBH and its definition based on a bulk density threshold has not been investigated.

Large-scale measurement of surface and canopy fuel characteristics using remote sensing data has been the subject of numerous studies and is becoming increasingly important for predicting fire behavior, assessing fire risk, or making management decisions. In this context, both passive (i.e., optical) and active (i.e., LiDAR and RADAR) remote sensing sensors are being used (Abdollahi and Yebra, 2023; Gale et al., 2021). The predictive ability of LiDAR instruments to describe the 3D-arrangement of vegetation is stronger for fuel loading and CBH compared to optical remote sensing products, even if limited for close to ground surface fuel due to occlusion issues (Bright et al., 2017). The vast majority of studies use classification approaches to map fuel metrics by training machine learning algorithms or performing multiple regression analyses with field data for a large number of LiDAR variables (Arkin et al., 2023; Just et al. 2022; González-Ferreiro et al., 2017; Jakubowksi et al., 2013; Marino et al., 2022). Depending on vegetation type, point density, classification methods, and the fuel metrics being predicted (e.g., surface fuel vs. crown fuel), the predictive power of these approaches is moderate to good for field data. However, training or calibrating these approaches requires a large amount of data that are laborious to obtain on the field and that are far from being error-free. Surprisingly, little attention has been paid to the potential of using the LiDAR point cloud to directly quantify fuel load and structural metrics. Direct estimates from the point cloud here refer to approaches that allow the spatial organization of the point cloud to be analyzed to extract meaningful metrics without using field data. However, there are a few notable examples, most of them using terrestrial LiDAR scans (TLS), which offer higher resolution and provide a fine description of the environment near the ground, but only operate at plot level (García et al., 2011; Wallace et al., 2022; Wilson et al., 2021). In these studies, the authors used TLS point clouds to extract CBH, FSG or fuel ladder metrics for describing the connection between surface and canopy but did not quantify fuel loading. Pimont et al. (2015) however proposed an approach to derive leaf bulk density profiles from TLS in mature *Quercus pubescens* forest. Chamberlain et al. (2021) used data from ALS to derive CBH at the tree level using a quantile method on the point cloud vertical distribution, and the Fire and Fuels Extension of the Forest Vegetation Simulator (FVS-FFE) to obtain CBD from CBH (i.e. thus indirectly).

Leaf area density (LAD) or plant area density (PAD), which refer to the one-sided leaf or plant area (when both wood and leaves are considered) per unit volume, are commonly used in forest ecology and management to describe vertical forest structure and can be derived from LiDAR data. Several theoretical approaches to derive PAD from TLS (Béland et al., 2014, 2011; Nguyen et al., 2022; Pimont et al., 2018) as well as from ALS (Bouvier et al., 2015; Lin and West, 2016) have been developed and described in the literature and are gaining attention. Several studies evaluated the potential of different methods to estimate leaf area index (LAI) in the field to derive CBD (Cameron et al., 2021; Clark and Murphy, 2011; Keane et al., 2005). However, to the best of our knowledge, vertical PAD profiles extracted from ALS data have never been used to derive bulk density vertical profiles at broad-scale and extract relevant fire fuel metrics, although they are closely related. However, several limitations are likely to restrict the practical application of such an approach. The point density of ALS data is much lower than TLS (roughly 10 pts m^{-2} versus thousands of pts m^{-2}) and the footprint diameter much larger, hence the description of the vegetation is impacted, especially near the ground where occlusion for ALS is high. In this context, Gale et al. (2021) highlighted that the vast majority of fire-oriented remote sensing studies, including ALS, focus on canopies because of poor vegetation description near the surface. Moreover, the limited description of a fine object with ALS data compared to TLS such as leaves, twigs or branches hinder the wood/leaf semantic segmentation of the point cloud, thus meaning the vegetation has to be considered as a whole while fuel is restricted to fine foliar and wood elements. Inversion of ALS point cloud in bulk density at different heights therefore presents several uncertainties and needs to be investigated.

This study aims at investigating the potential of ALS to directly estimate several metrics describing fuel load in different strata and its vertical continuity. We have developed a method to i) derive the vertical profile of PAD from the ALS point cloud inspired by previous work on radiative transfer inversion and LiDAR data, ii) convert the vertical PAD profile into vertical bulk density profiles using species-specific plant traits, and iii) derive fuel metrics from the vertical bulk density profiles

that can be mapped at broad scale. The approach is evaluated in two specific steps using field data from France, Spain, and Portugal, on a wide variety of forest plots. More specifically, we evaluate i) the ability of LiDAR to describe vertical vegetation density profiles from the ground to the top of the canopy, and ii) the agreement of ALS-based fuel metrics extracted by our method with fuel metrics derived from field-based approaches. Moreover, the sensitivity of several parameters of our methods is assessed to analyze the importance of considering the vegetation types (i.e. species) and structure, as well as to recommend a set of optimal parameters for broad-scale applications. Finally, we highlight the limitations of LiDAR and field data in describing fuel load and fuel vertical distribution.

2. Materials and methods

2.1. Dataset

Field and ALS data from southeastern France, Spain, and Portugal were used. While French field data allowed us to evaluate the ability of ALS data to describe vertical vegetation profiles from ground to canopy top, Portuguese and Spanish data were used to evaluate several metrics related to canopy fuels (i.e. CBH, CFL and CBD).

2.1.1. Field data

2.1.1.1. Vertical fuel stratification measurement (Southeastern France data). Field data used to assess the ability of ALS point clouds to describe the vertical vegetation profile were collected in 2022 by the French National Forest Service (ONF) on 296 10-m radius plots in southeastern France. Plots were sampled within a variety of forest types representative of the diversity of vegetation types in French Mediterranean ecosystems (Fig. 1), with 24 different dominant species and plot heights ranging from 0.5 m to 44 m with an average height of 14.7 m (Table 1 and Table S1).

Vegetation cover was estimated in seven layers (i.e., 0–0.5 m; 0.5–1 m; 1–2 m; 2–3 m; 3–4 m; 4–5 m; and > 5 m) on each plot. A team of two field operators estimated visually the percentage of vegetation cover in each layer. Layer limits were estimated after training and calibrating body parts height (e.g. knees, hips, breast, head) or by using graduated poles when uncertain. Vegetation surface projection is not straightforward to estimate visually on the field at different heights, but French National Forest crews have been trained with inter-evaluation exercises to limit operator bias. Moreover, to facilitate visual estimation, each layer was divided in four quarters, respectively east to north, north to west, west to south and south to east, and the cover was separately

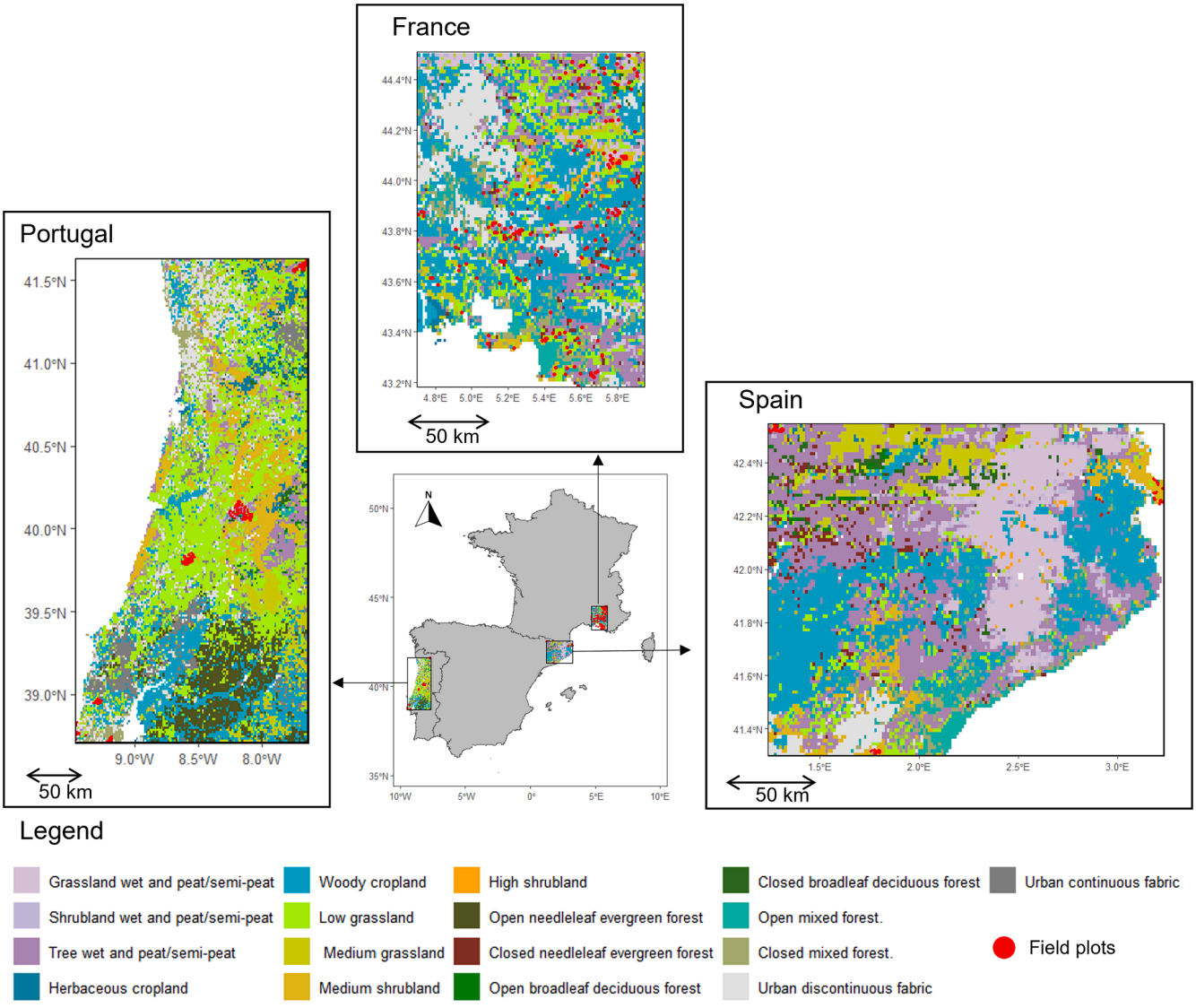

Fig. 1. Plot location in France, Spain and Portugal (red dot). LiDAR data are available for all the plot locations. The colored map in the sampled zone comes from the European fuel map (Aragoneses et al. 2023) summarize by country.

Table 1
Field and ALS data summary.

Country	N plots	Plot radius (m)	Height (m)	Field data	Field campaign date	ALS density (pts/m^2)	ALS acquisition date	ALS device	Data owner
France	296	10	14.7 (0.5–44)	Vegetation Cover in 7 strata	2022	65 (8.3–203)	05–09/ 2022	Leica TerrainMapper 2	IGN (Publicly available)
Portugal	409	12.62	16.6 (3.3–40.3)	CBH DBH CFL$^+$CBD$^+$ Height	04/2020 06/2021	16.2 (4.5–73.6)	06/2020	Teledyne Galaxy. SwathTrack	ICNF (Publicly available)
Spain	140	10	14 (1.8–34.8)	CBH	07–09/2023	22 (10.4–44.8)	2021–2023	Leica TerrainMapper 2	ICGC (Not Publicly available)

*CBH = Crown base height in m; DBH = diameter at breast height in cm; CFL = Canopy Fuel load in kg/m^2, CBD = Canopy bulk density in kg/m^3.
*IGN: French National geographic institute; ICNF: Portuguese Institute for Nature Conservation and Forests; ICGC: Catalan cartographic and geographic institute.
$^+$ Calculated from allometries based on field inventory.

estimated in each quarter. The mean of the four cover values was used. The percentage of vegetation cover was estimated in tenths. Even if the measurement is coarse, the objective was to obtain quantitative data over a large set of forest types, to compare LiDAR estimates to the forester's perception of fuel density and distribution. This protocol is relevant to compare ALS and field data for vertical fuel stratification in forest stands (Marino et al. 2018). Diameter at breast height (DBH), species, and tree spatialization using azimuthal angle and distance from the plot center were also recorded for every tree larger than 7.5-cm DBH. The plots were geo-located using a Trimble GPS on a tripod with a precision of 1–3 m. Postprocessing consisting of a manual match between the spatialized field inventory and the digital height model extracted from the ALS point cloud allowed precise correspondence between field plot and ALS data.

2.1.1.2. Canopy fuel property measurement. Portuguese data were acquired for six areas with various forest types (Fig. 1). In these areas, 409 circular plots with a radius of 12.62 m (500 m^2) were sampled (Mihajlovski et al., 2023). Tree height, crown base height, and the diameter at breast height (DBH) of each tree within a plot were measured and tree species was recorded, the plots being dominated by 14 different species (Table S1). These metrics were used for estimating canopy fuel load (CFL) and canopy bulk density (CBD) from species-specific allometries for leaf fraction of biomass using the Portuguese National Forest Inventory (PNFI) equations (Tomé et al., 2007) and general allometries for thin wood element fraction (Gómez-Vázquez et al., 2013). These data were acquired between April 2020 and June 2021. Plots were geo-referenced with sub-metric precision using a TRIMBLE Juno Handheld (Trimble Inc. USA) with external antenna.

Spanish data consist of 141 plots with a 10-m radius distributed across four different ecological areas in Catalonia. 38 plots were sampled along the inland northern Mediterranean coast; 38 along the inland central Mediterranean coast; 45 plots in the Pyrenees and 20 plots in a riparian vegetation area (Fig. 1). These plots are dominated by 16 different species of which nine are the most common tree species in Catalonia (Table S1). For each plot, number of trees and their species were recorded and their crown base height was measured. The plots were geo-referenced using a Leica Zeno FLX 100 GPS, with a precision of 2–3cm.

2.1.2. LiDAR data

The French National Geographic Institute (IGN) is currently conducting a national-scale high resolution ALS campaign that started in 2021 and will end in 2025. These ALS data are publicly available and can be downloaded from the IGN platform ("LiDAR HD | Géoservices," 2024). ALS data collected from May to September 2022 were used as it matches the period of field data campaign and correspond to leaf-on phenology. The 296 field plots (10-m radius) were extracted from the point cloud. The data were acquired by a Leica TerrainMapper 2 at an average point density of 65 m^{-2} per sampled plot (Table 1).

LiDAR from Portugal were acquired in June 2020 within the six target areas described in the field data section. These data are publicly available and provided by ICNF (Institute for Forest and Nature Conservation). The data were acquired using a Teledyne Galaxy Airborne LiDAR with SwathTRAK Technology with an average point density of 16.2 m^{-2} per plot.

The Cartographic and Geographical Institute of Catalonia (ICGC) completed the acquisition of the 3rd Catalan LiDAR coverage (LIDARCAT3) from 2021 to 2023, covering the whole territory of Catalonia (Spain). The data was collected by a Leica Terrain Mapper 2. Out of a total of 141 plots, 121 were extracted from LIDARCAT3. The remaining 20 plots were extracted from another ICGC flight with the same LiDAR system. LiDAR data for the 45 plots in the Pyrenees were acquired between October and November 2022, during the leaf-off conditions of deciduous trees. LiDAR data for the other plots were acquired between April and July 2021.

All point clouds were provided in .laz format. The point cloud classification was made by IGN, ICNF and ICGC for France, Portugal and Spain respectively. Only classes 2 to 5 corresponding to ground and vegetation were used.

2.2. Processing of LiDAR data

All the ALS data processing was performed in R. The workflow is implemented in an R package called LidarForFuel available on a github repository (see code availability section) that can be used with the lidR package allowing broad-scale LiDAR treatment (Roussel et al., 2020a). Preprocessing steps consist of:

(i). Point cloud filtering for keeping only ground and vegetation points (LAS classes 2 to 5). A SOR (statistical outlier removal) filter with conservative parameters ($k = 5$ and $m = 10$; see lidR package for details on the filter function parameters) was applied to remove lost points well above the canopy or well below ground that can remain from the initial classification provided.

(ii) Normalizing the height of the point cloud using a spatial interpolation algorithm (with k and m parameters of 5 and 10 resp.) based on Delaunay triangulation over points classified as ground category (Fig. 2 Step 1 and 2).

2.2.1. LiDAR data processing for extracting fuel metrics

2.2.1.3. ALS point cloud to vegetation density profile (Fig. 2 step 3). Normalized return density index (NRD) is widely used to describe the vertical profile of vegetation density from ALS data as it takes into account occlusion (i.e. attenuation of the laser beam by the canopy) when calculating the proportion of returns in a given layer. (Campbell et al., 2018; Forbes et al., 2022; Kane et al., 2013; Marino et al., 2018). It is calculated as follows:

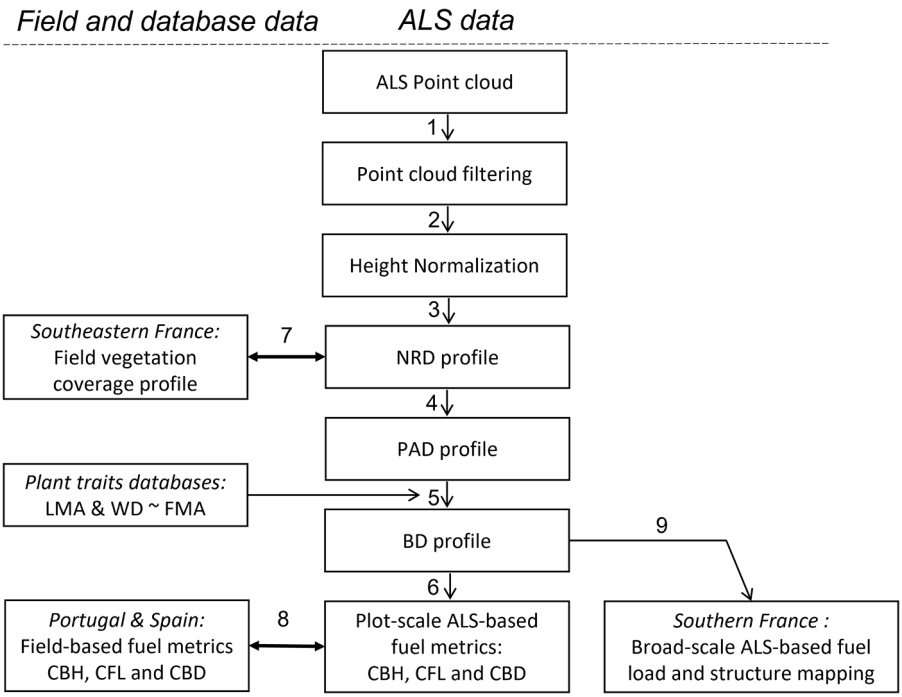

Fig. 2. Summary of the workflow. The numbers correspond to the step of the workflow reference in the text. The bold double arrows refer to the analysis for comparison between field and ALS data (step 7 and 8). Step 9 consist in mapping fuel metrics at broad scale at 20 m resolution raster. References to the steps are given in section headings. LMA: Leaf Mass Area (kg/m^2); WD: Wood Density (Kg/m^3); FMA: Fuel Mass Area (Kg.m^2) CBH: Canopy Base Height (m), NRD: Normalized Return Density; PAD: Plant Area Density (m^2/m^3); CBD: Canopy Bulk Density (Kg/m^3); BD: Bulk Density (Kg/m^3); CFL: Canopy Fuel Load (Kg/m^2).

$$NRD = \frac{N_i}{N_{0-i}} \quad (1)$$

where N_i is the number of returns in layer i and N_{0-i} is the number of returns in layer i and below (i.e. from the ground to the top of layer i).

2.2.1.4. ALS point cloud to plant area density (Fig. 2 step 4). PAD_i was estimated based on the general approach consisting of using the Beer-Lambert law (i.e. law of light extinction in a turbid medium) extended to plant canopies by Monsi and Saeki (2005), for deriving plant area from the transmittance $P(\theta)$ of a volume from a viewing angle Θ:

$$P(\theta) = e^{((-G(\theta).PAD_i.\Omega)/(cos\ (\theta)))} \quad (2)$$

where θ was estimated by calculating the beam angle using the trajectories of the plane. The trajectories of the plane were reconstructed using the point cloud with Roussel et al. (2020b) algorithm with lidR R package. $G(\theta)$ is the plant projection ratio from a viewing angle θ. We assumed a spherical distribution of leaf inclination angles within canopies, with $G(\theta)$ value well approximated by 0.5 (half of the leaf surface) (Ross, 1981).

Finally, Ω is the clumping index describing the aggregation of vegetation. Ω =1 assumes a homogeneous distribution of plant elements that is very unlikely at our scale of analysis (10 to 12.62-m plot radius or 20-m x 20-m pixels) and more likely varies from 0.55 to 0.86 according to the literature (Chen et al., 2005). A value of 0.77 was retained based on a sensitivity analysis of Ω that allowed us to find the optimal Ω, reducing the bias between field and ALS fuel load estimation. This analysis is described in Appendix 1.

The transmittance $P(\theta)$ is considered equal to the gap fraction (Gf) that is estimated from the point cloud (Bouvier et al. 2015) in a specific layer i by:

$$G_{f_i} = 1 - NRD_i \quad (3)$$

From Eq. (2) and (3), the Plant Area Density (PAD, in m^{-2} m^{-3}) within the vegetation layer *i* in which NRD is computed is then approximated by:

$$PAD_i = -\frac{ln(G_{f_i}).\cos(\theta)}{G(\theta).\Omega.D_i} \quad (4)$$

where $D_i$is the depth of the vegetation layer i

2.2.1.5. PAD to bulk density profile (Fig. 2 step 5). We assume that above the ground, most of the laser beams are intercepted by fine fuel elements (i.e. leaves, needles, small twigs), which comprise most of the projected vegetation area. The bulk density profile can thus be derived from multiplying the PAD profile by the Fuel Mass Area (FMA), i.e., the mass of canopy fuel per unit area (in kg m^{-2}).

FMA mostly depends on the mass fraction of leaf elements with respect to fine fuel elements - typically corresponding to elements thinner than 6 mm - α_L, the Leaf Mass Area (LMA) and the Twig Mass Area (TMA).

$$FMA = \frac{1}{\frac{\alpha_L}{LMA} + \frac{1-\alpha_L}{TMA}} \quad (5)$$

LMA and TMA vary widely among tree species and forest types. We used species-specific LMA and TMA according to the dominant species of each plot. LMA values were extracted from the global spectrum of plant form and function dataset (Díaz et al., 2022).

TMA is by far less well-known than LMA, so we used simple rules of thumb to estimate it. As TMA is representative of 0–6 mm diameter elements, we considered an average of 4 mm, as the amount of 0–2 mm is negligible compared to the 2–6 mm amount. The species-specific wood density (WD in kg m^{-3}) is finally used and a half-cylinder surface is considered for deriving TMA following:

$$TMA = WD\ r \quad (6)$$

with r being the radius of twigs considered (r = 0.002 m). Species-specific WD values were extracted from three different databases depending on the availability of a given species, the xylem functional

trait database (Choat et al., 2012) or the global wood density database (Chave et al., 2009), or the global spectrum of plant form and function dataset (Díaz et al., 2022).

α_L was estimated from destructive field data obtained on the three tree species dominating the Mediterranean forests of southeastern France (i.e. *Quercus pubescens, Quercus ilex* and *Pinus halepensis*). Field samples were collected in 2016 for 14 individuals with a wide range of crown diameter, height and foliar density (Soma, 2019). Whole trees were destructively sampled from top to bottom. Each tree was divided in 1-m vertical strata, and for each strata the weights of twigs and leaves were measured. The twigs (0–6 mm diameter) and leaves mass fraction (α_L) resulting from this field campaign are summarized in Table 2. This type of data is not common and hard to obtain at species level so we used a constant α_L value of 0.51, the average of the three species. The bulk density profile was computed for each French, Spanish and Portuguese plot from the PAD profile.

$$BDij = PADij\ FMA_j \quad (7)$$

where *BDij* and *PADij* are respectively the bulk density and PAD value of strata i in the plot j; FMA_j is the dominant species-specific FMA value of plot j.

2.2.1.6. Bulk density profile to LiDAR-based fuel metrics (Fig. 2 step 6). Bulk density profiles can exhibit different forms with several vegetation strata. Five stratum height boundaries and the corresponding four stratum were identified for deriving fuel load and fuel vertical organization metrics (Fig. 3). Description of stratum and rationale behind the segmentation as well as fuel load metrics extracted are described in Table 3. Identification of stratum's limits depends on a bulk density threshold that can be defined as the critical amount of fuel that allows fire transmission to the crown (see section 2.3.4).

Note that apart from the fuel load metrics other important fuel characteristics are derived from those profiles:

- Canopy height (CH) in meters: maximum height of the profile
- Canopy base height (CBH) in meters: lowest height of the canopy stratum above a given bulk density threshold
- Canopy bulk density (CBD) in kg m^{-3}: ratio between CFL and crown length (i.e. CH – CBH)
- Fuel strata gap (FSG) in meters: depth of the gap strata (Fig. 3)

In addition to these quantitative metrics a qualitative fuel profile type (FPT) metric describing the shape of the bulk density profile was also extracted (Fig. 3, II). Four specific FPT were identified on a gradient of vertical complexity which is based on the number of fuel stratum separated by gaps. A gap is considered if the depth of the stratum with bulk density lower than a threshold (i.e. 10 % of the maximum bulk density) is larger than 1-m height. Due to larger uncertainties below 1 m, the elevated surface fuel stratum is not considered for characterizing the FPT which is therefore computed from 1-m height to the top of the canopy.

- "A": The simplest profile with canopy stratum only (e.g. archetype of a mature pine plantation without midstory).
- "B": A midstory and a canopy stratum separated by a fuel strata gap (e.g. a dominant canopy species and a shrub stratum; pine plantation with shrub/fern understory) corresponding to the example used in Table 3 for illustrating all potential strata.
- "C": Complex multi-layered forest (e.g. uneven-aged and/or diverse forest stand; mixed unmanaged forest, shrubland)
- "D": The vegetation is continuous (e.g. dense mixed unmanaged forest, closed shrubland). In this last case CBH and the FSG do not exist and are equal to 0, the canopy and the continuous midstory strata are connected. The CFL is therefore equal to 0.

Schematic representations of the FPT and examples of real-world profiles extracted from Portuguese data are given on Fig. 3 but see Appendix 2 for more examples and detailed explanations of real-world profiles.

Table 2
Twigs and leaves mass fraction measured on the field for three Mediterranean tree species.

Species	Twigs mass Fraction	Foliar mass fraction (α_L)	N samples	N trees
Quercus pubescens	0.47	0.53	35	5
Quercus ilex	0.47	0.53	18	5
Pinus halepensis	0.53	0.47	23	4

2.3. Data analysis

2.3.1. Evaluation of the consistency between NRD and field vertical coverage profiles (Fig. 2 step 7)

Field vertical coverage profiles (i.e. French plots field protocol) were compared to ALS-based vegetation density profiles (i.e. NRD profiles) to control for the consistency of ALS data with fuel density perception of foresters on the field. Regressions between NRD and field vertical coverage profiles (i.e. French field plots) were therefore analyzed. However, field coverages cannot be considered as direct estimates of fuel density. Indeed, bulk density within crowns varies depending on species (Armand et al., 1993; De Cáceres et al., 2019), but also on stand structure, where taller stands with strong competition for light and lengthier crowns tend to exhibit lower bulk density. Therefore, we expect a different relationship here with a slope decreasing with vegetation density. Uncorrelation between ALS-based and field-based vegetation profiles would be interpreted as ALS failing to represent vegetation density due to imprecision in LiDAR data (e.g. low point density, occlusions, point classification issues).

To match the French field protocol, *NRD* was calculated in the same seven strata of varying depth (i.e., 0–0.5 m; 0.5–1 m; 1–2 m; 2–3 m; 3–4 m; 4–5 m; and $>$ 5 m).

2.3.2. Evaluation of ALS canopy fuel metrics (CBH, CFL and CBD) against field canopy fuel data (Fig. 2 step 8)

Three-fuel metrics (CBH, CFL and CBD) were estimated from the point cloud of all the 409 Portuguese plots and CBH for the 140 Spanish plots and then compared to field data (Fig. 2). The bulk density profiles were calculated for constant 0.5-m stratum depth. CBH definitions are different between i) the LiDAR-based approach, which uses a CBD threshold on the vertical bulk density profile consistently with the fire-behavior "concept" of CBH described in the Introduction, and ii) the forestry CBH which is the average field value of individual crown base heights (height of first living branches). Hence, for calculating CFL and CBD based on ALS data, the field CBH and mean tree height were used to ensure that the fuel loads are compared in the same stratum boundaries.

Relationship between ALS and field-based estimates were analyzed for each FPT described on Fig. 3 II. It is expected that the simpler the profile the more comparable the metrics are between ALS and the field. In particular, the concept of FSG or CBH based on threshold of bulk density for FPT "D" is not relevant as fuel is continuously high in the whole stratum and results in CBH = 0 (cf Fig. 3 and section 2.2.1.4). In this case of vertical continuity a "forestry" CBH can still be measured, which illustrates the discrepancy between the two concepts. See Appendix 2 (Fig. A2) for a comparison and explanation of ALS-based and field-based CBH on real-world profiles.

Consistency between field and ALS-based estimates was assessed using the following statistics:

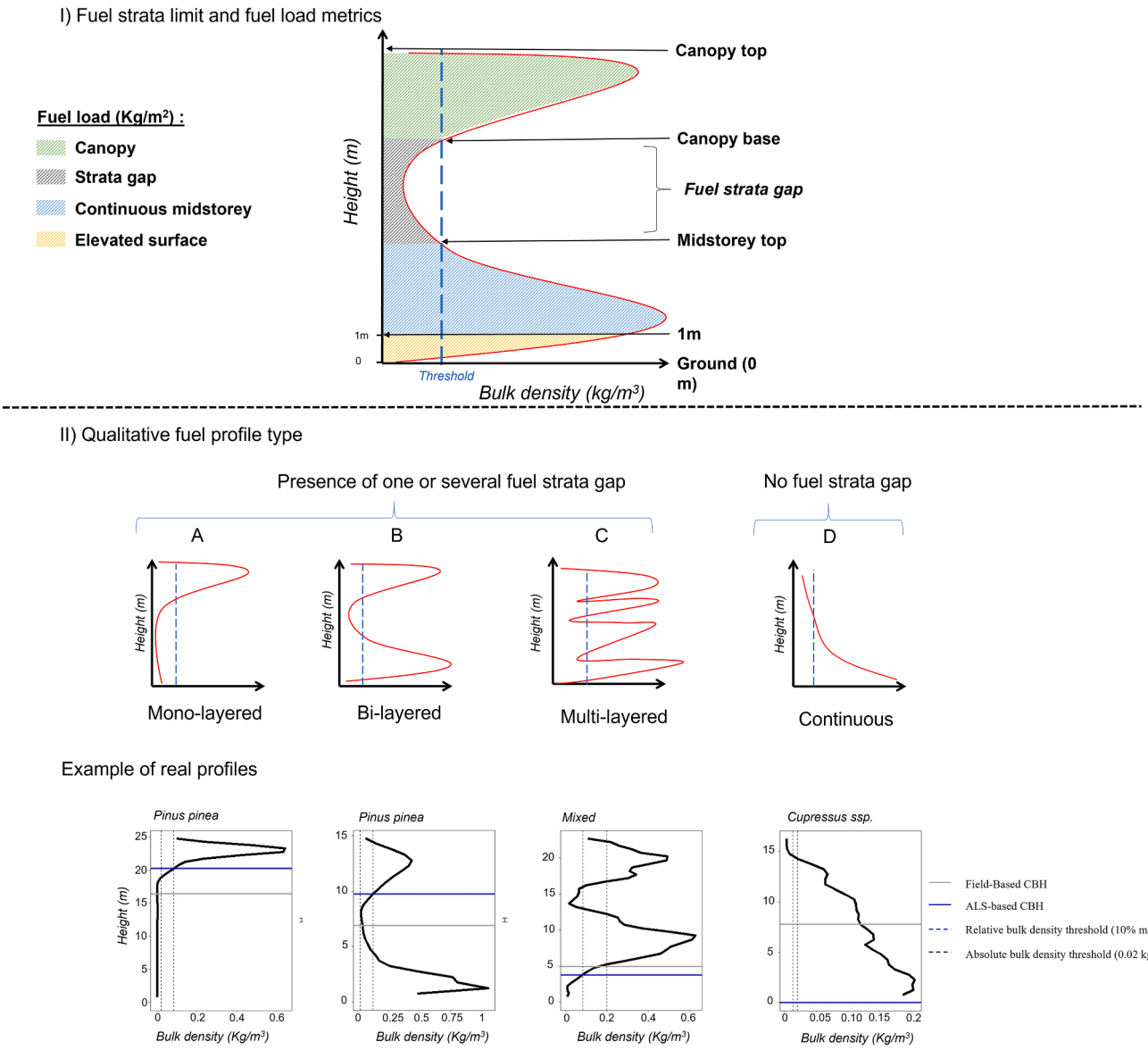

Fig. 3. I) Schematic representation of a vertical bulk density profile extracted from ALS point cloud illustrating the five potential strata's limits identified based on a bulk density threshold and the corresponding four fuel load metrics of the strata (see Table 3 for a description of the strata). The dashed blue line corresponds to a bulk density threshold used to identify the strata's limits. II) Schematic representation of the four-fuel profile type (FPT). The blue dashed lines correspond to a relative threshold (i.e. 10 % of maximum bulk density) used to identify the profile type. Note that the red profiles are theoretical and examples for real-world plot profiles are given below. More real profiles and explanations are given in Appendix A2.

$$R^2 = 1 - \frac{\sum_{i=1}^{n}(\hat{y}_i - y_i)^2}{\sum_{i=1}^{n}(\hat{y}_i - y_i)^2} \quad (8)$$

$$RMSE = \sqrt{\frac{1}{n}\sum_{i=1}^{n}(\hat{y}_i - y_i)^2}, \quad (9)$$

$$nRMSE\ (\%) = \frac{RMSE}{mean(\hat{y})} * 100, \quad (10)$$

$$bias = \frac{1}{n}\sum_{i=1}^{n}(\hat{y}_i - y_i), \quad (11)$$

$$nbias\ (\%) = \frac{bias}{mean(\hat{y})} * 100 \quad (12)$$

where n represents the number of plots, y_i is the field-based fuel metric of $plot_i$, $\hat{y}_i$ is the ALS-based metric of $plot_i$, and $\bar{y}_i$ is the mean of the field-based metric.

2.3.3. Analyzing the sensitivity to species-specific traits

To analyze the contribution of species-specific plant traits used in our ALS-based methods, CFL and CBD estimated for the 409 Portuguese plots were computed with and without species-specific traits and compared between each other and with field-based CFL and CBD. Without species-specific traits, average LMA and WD field values of the Portuguese plots were used (0.14 kg m^{-2} and 591 kg m^{-3} respectively) resulting in a constant FMA of 0.25 kg m^{-2}. Only species dominant in >10 plots were analyzed. Differences between ALS-based metrics (i.e. CFL and CBD) with and without species-specific traits were analyzed with a non-parametric mean comparison statistical test. The same approach was used to analyze the differences between field-based and ALS-based metrics (with and without species-specific traits).

Table 3
Description of the four potential strata identified from ALS based on a bulk density threshold. Depending on the fuel types, they can contain only the lower one (e.g. grassland or low shrubland), the first two (e.g. high shrubland, immature or mixed stand) or the four of them (e.g. mature forest with low density midstory).

Profile scheme	Strata limits	Strata name	Description	Fuel load metrics (kg/m²)
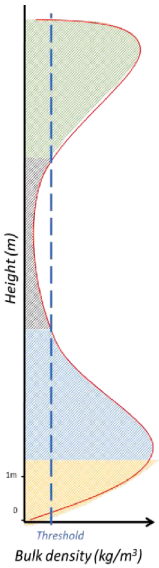	Canopy base height – top canopy	Canopy	The canopy fuel strata, above the fuel strata gap	**CFL**: canopy fuel load
	Midstory top height – Canopy base height	gap	Correspond to the strata gap fuel (in case there is a gap) which is the fuel with bulk density lower than the threshold (blue dashed line on the profile scheme). This fuel should be accounted in fuel consumption in case of crowning in the canopy fuel strata	**SGFL :** strata gap fuel load
	1m- midstory top height	midstory	Stratum higher than 1m and connected continuously to the elevated surface fuel (ie bulk density higher than threshold) according to a bulk density threshold. It can contain upper parts of surface fuel and shrubs (>1m), ladder fuel, midstory and even the crowns in case of vertical continuity with the canopy.	**MFL** : midstory fuel load
	0-1m	Elevated surface	This strata depth is constant (i.e. 1m) and therefore independent from the bulk density threshold used. Fuel load characterization in this stratum with ALS likely present uncertainties (especially in 0-0.5m) due to occlusion and ground confounding effect (see Result and Discussion section)	**ESFL** : Elevated Surface Fuel load

2.3.4. *Analysis to identify an absolute bulk density threshold*

ALS-based CBH identification for estimating and mapping canopy and understory fuel characteristics requires setting a specific absolute bulk density threshold that corresponds to the critical amount of fuel that allows fire transmission (Sando and Wick, 1972; Scott and Reinhardt, 2001). Several threshold values have been proposed in the literature (Reinhardt et al., 2006; Cruz and Alexander, 2010), but are not systematically based on fire physics and are subject to many uncertainty sources. Therefore, a bias analysis between field-based and ALS-based CFL and CBH for twenty different bulk density thresholds ranging 0.01 to 0.1 kg m^{-3} was performed to find a threshold that could be used with our ALS-based approach for mapping canopy fuel metrics at broad scale. The threshold minimizing the CFL and CBH bias was retained. Note that this recommendation is based on field (for CBH) or field-derived (for CFL) metrics and not on fire physics considerations. The detailed sensitivity of ALS-based metrics to twenty different bulk density thresholds is described in Appendix 3.

3. Results and discussion

3.1. *Evaluation ALS vertical vegetation profile with field data*

Vegetation coverage estimated on the field has been used for evaluating, rather than validating, the ability of the NRD index to describe vegetation vertical profile. This type of data is indeed difficult to obtain on the field and by no means free of errors. It is still a good point of comparison to identify obvious problems in ALS-based vertical profiles.

Moderate to good relationships (R^2 from 0.39 to 0.70) were systematically found for stratum above 0.5 m (Fig. 4). The weak (but still significant) relationship found between field vegetation coverage and the ALS estimate of vegetation density in the lowest stratum (0–0.5 m) with a R^2 of 0.11 (Fig. 4) was expected (Bright et al., 2017; Jakubowksi et al., 2013). It can be explained by the limits of ALS to describe near-ground vegetation because of the occlusion. The highest stratum hides the vegetation elements of the lowest, leading to a poor description of these strata, and the ground/vegetation classification issues decreases accuracy in the estimation of the vegetation return (Ni) close to the ground that is involved in NRD estimation. Campbell et al. (2018) reached a R^2 of 0.44 between NRD and field cover estimate close to the ground strata but they considered a single stratum from 0.15 m to 1.85 m. Overall, our results are encouraging considering that previous studies describing vegetation for fuel characterization with lower density ALS data (1 to 5 pts m^{-2}) focused only on middle canopy (from 2 m or even 4 m) to avoid large uncertainties below (Kramer et al., 2014; Marino et al., 2016). We thus argue that above 0.5 m, high-resolution ALS data (Table 1) can reliably describe the vertical distribution of vegetation using the NRD index as already suggested by Marino et al. (2018) for classifying presence/absence of ladder fuels. Finally, seasonal changes of low vegetation due to the annual phenology cycle can also explain the poor relationships in close to ground strata. Most of the field data were collected during autumn and winter while LiDAR data were acquired during spring and summer. Small differences in the data collection period (a few months) can result in height and cover variations for herbs and forbs.

Fig. 5 illustrates the relationship between NRD in the lowest stratum (0–0.5 m) and NRD in the second stratum (0.5–1 m). If the NRD of the first stratum contained no information about the amount of biomass present, but only residual noise due to soil-vegetation confusion, then there would be little or no correlation between NRD values in these two strata. On the contrary, the high correlation observed between the NRD of the first two strata ($R^2 = 0.60$) is consistent with the fact that vegetation in the second stratum contains structural elements of the first stratum by construction. This suggests that the poor relationship between field cover and NRD in the close to ground strata could not only be due to a lack of data or classification problems with ALS but might be also due to a time lag (even if small) between the two sources of data and that ALS descriptions in the lowest strata might be reliable. However, we have no means for evaluating the respective contributions to our results of ALS limitations and acquisition lag. To disentangle these two effects, data must be collected at the exact same phenological period. Therefore,

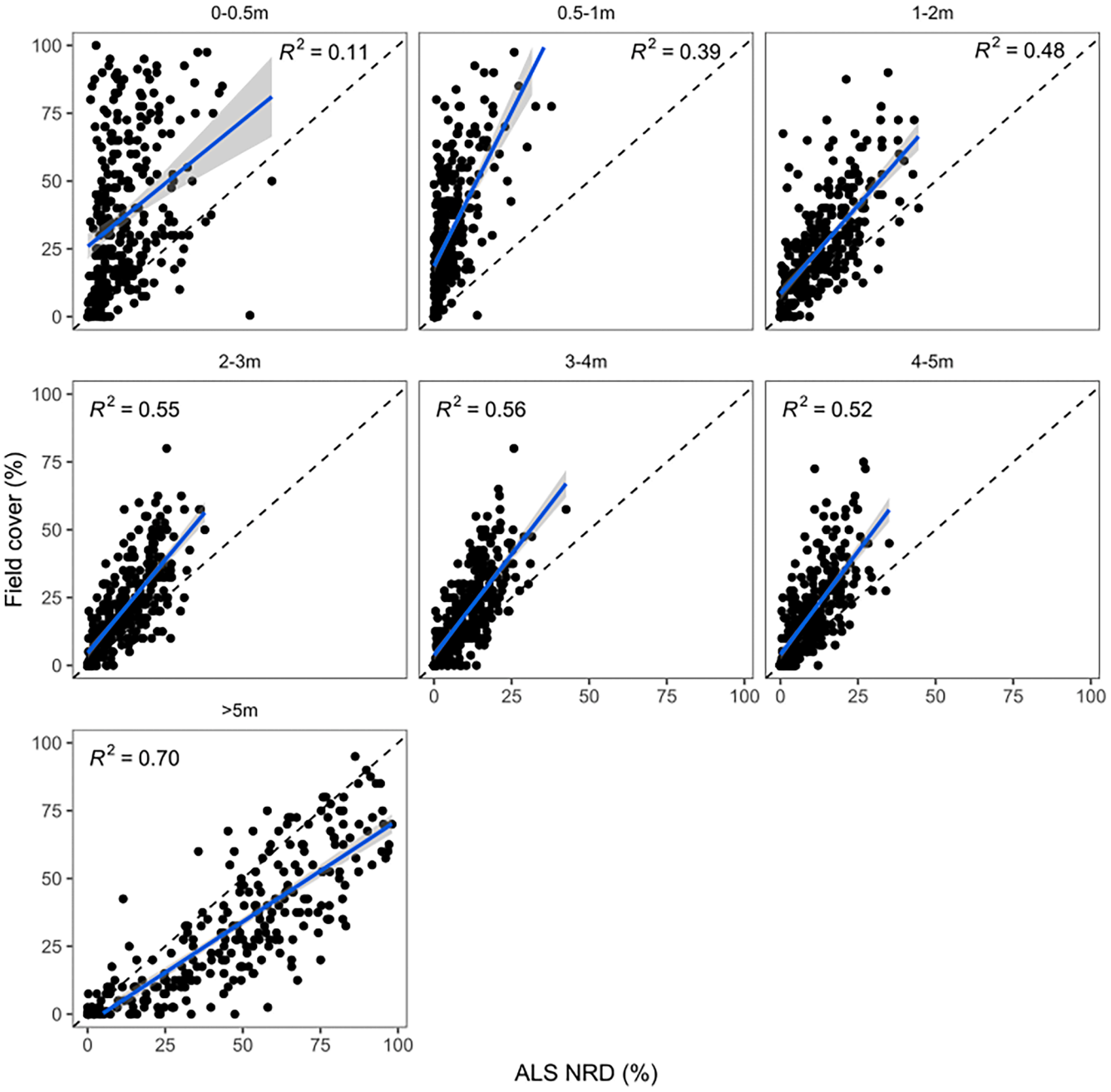

Fig. 4. Relationship between field cover and NRD for each layer assessed on the field. The blue line represents the linear regression and the grey shaded area represents the 95 % confidence interval. R^2 of the linear regression are indicated on each graph to indicate the goodness of fit. The dashed line represents the 1:1 line.

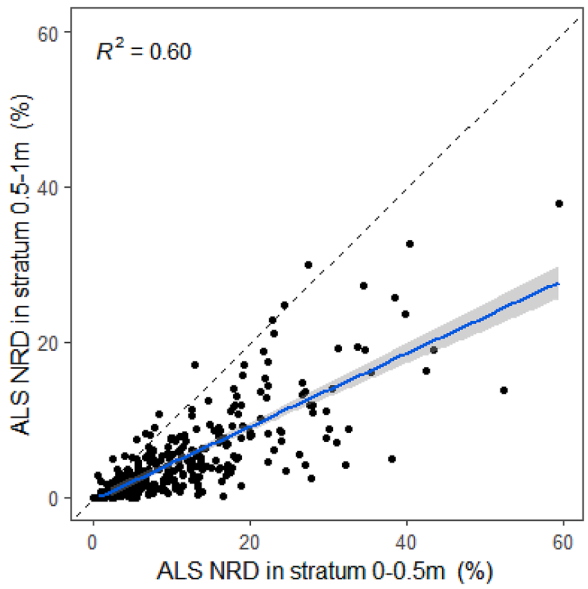

Fig. 5. Relationship between NRD in the lowest strata (0–0.5 m) and NRD in the second stratum (0.5–1 m). The blue line represents the linear regression and the grey shaded area represents the 95 % confidence interval. The dashed line represents the 1:1 line.

fuel load of the elevated surface stratum (i.e. 0–1 m) have to be used and interpreted with caution. Considering the importance of surface vegetation to fire ignition and spread, an effort has to be made to assess the uncertainties of high-density ALS data in this stratum and improve our ability for describing surface fuel. Combining high-density ALS and other remote sensing products that are available at high frequency seem also promising for characterizing this specific stratum (Labenski et al., 2023).

Overall, NRD underestimated the field vegetation cover (Fig. 4). This result is consistent with previous studies (Marino et al. 2018) and with the fact that some of the lidar beams hitting vegetation clumps can pass through them. So, the lighter the vegetation in the clumps, the more the NRD tends to underestimate ground cover. The case of the >5-m stratum is specific, vegetation density being higher in this stratum compared to others (0.5 or 1 m), as the stratum combines all vegetation >5m (height is generally >6m). This could explain why the slope is almost equal to 1 in the latter case.

3.2. Evaluation of ALS canopy fuel metrics with field data

3.2.1. Canopy base height (CBH)

A critical aspect of the results comparing ALS and field-based fuel metrics resides in the divergence of CBH definition between the two approaches. ALS-based CBH estimation is based on a critical amount of fuel in the canopy to spread fire, i.e. a wildfire-oriented definition (Sando and Wick, 1972), while field-based estimation is based on the average height of the first live branches of the trees (i.e. a general forestry definition).

Fig. 6 shows the relationship between ALS-based and field-Based CBH. Identifying a simple vertical profile (i.e. Profile type "A") reduced the differences between the two definitions and resulted in a good relationship between field-based and ALS-based CBH (R^2 = 0.6, nRMSE = 42 % and nbias = 5 %). *Pinus pinea* and *P. pinaster, Eucalyptus globulus* and *Quercus suber* stands represented most of the profile type "A" and are thus characterized by even-aged stands with a well-defined monolayered canopy with very low inter-individual CBH variability inside a plot (*sensu* field data) (Fig. 3 and Fig. A2). The threshold used to estimate ALS-based CBH is relative and has no rationale in terms of fire physics but revealed that in a simple structure stand, where an actual canopy base can be identified at the plot level, ALS can reliably estimate a field-based CBH. However, as expected, no correlation was found between ALS-based and field-based CBH in more complex profile types (i.e. the bi-layer profile "B" and the multi-layer profile "C" in Fig. 6). The profile type "D" is not shown in Fig. 6 as the continuous profile has an ALS-based CBH always equal to 0 and thus was uncorrelated with field-based CBH. In these three types of complex and continuous stands (B, C and D) the CBH field definition at the stand scale is less meaningful in the context of fire risk and behavior. We argue that for that kind of complex or continuous forest structure our approach describing full bulk density profiles is much more relevant and accurate for mapping canopy fuel metrics at regional scale than using classification approaches based on the field definition of CBH. The example of bulk density profiles in Appendix 2 illustrates how CBH estimated from ALS and field can match in a specific context (mono-stratified stands) and how in other contexts the field definition of CBH is less relevant for wildfire behavior purposes while ALS profiles are much more informative.

3.2.2. Fuel load metrics

In most studies, including in the present work, field-based estimates of CFL and CBD come from allometric models developed from limited destructive sampling (Cruz et al., 2003; Fernández-Alonso et al., 2013). Allometries are known to be subject to large uncertainties related to

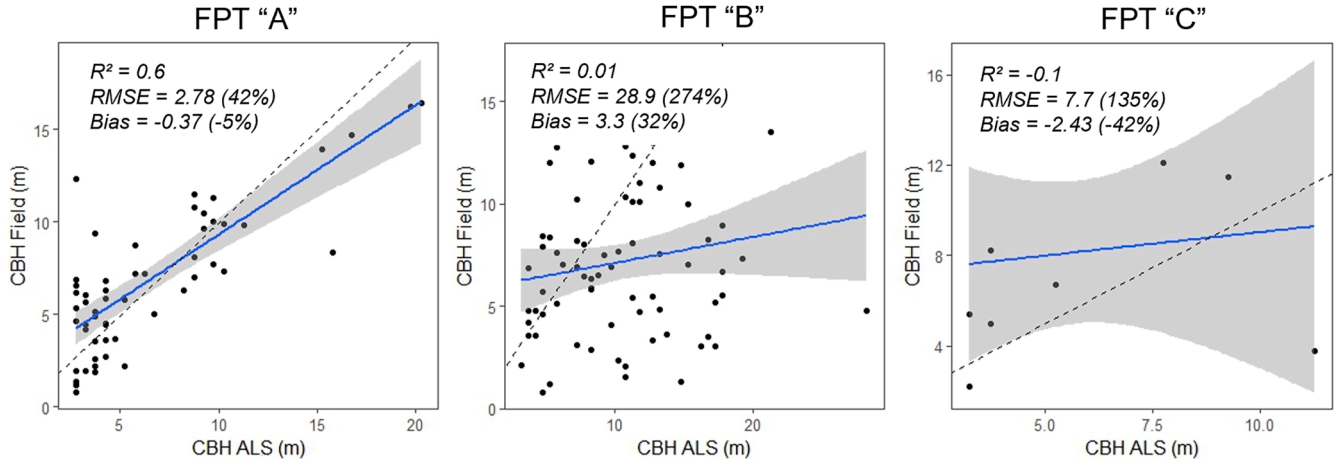

Fig. 6. Linear regression between field and ALS-based CBH for each of the three-profile type estimated. Statistics of the regression are given on the graphics. In brackets are the normalized values of the statistics (i.e. nrmse and nbias). ALS-based CBH of profile type "D" is always equal to 0, the relationship is therefore not drawn. The blue line represents the linear regression and the grey shaded area represents the 95 % confidence interval. The dashed line represents the 1:1 line.

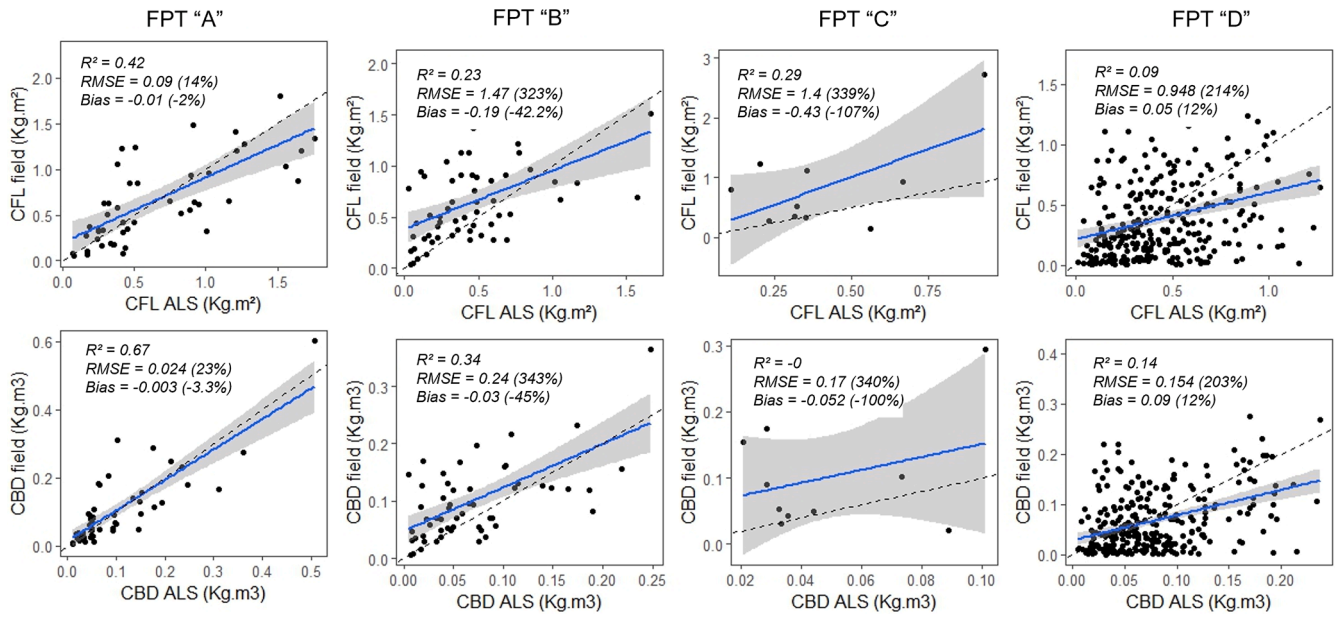

Fig. 7. Linear regression between field and ALS-based CFL and CBD estimates for each of the three-profile type estimated. Statistics of the regression are given on the graphics. In brackets are the normalized value of the statistics (i.e. nrmse and nbias). The blue line represents the linear regression and the grey shaded area represents the 95 % confidence interval. The dashed line represents the 1:1 line.

biotic (e.g., competition) and abiotic (e.g., soil properties) factors (Lines et al., 2012) and are highly dependent on species (De Cáceres et al., 2019), but also to factors that are less straightforward to measure such as tree age (Shaiek et al., 2011). However, non-destructive sampling is the primary method for estimating those fuel properties from field data because of the labor-intensive nature of harvesting and processing biomass. Mapping fuel load estimates at broad-scale and high resolution (e.g. 20 m) directly and accurately from remote sensing data is therefore a major challenge . The recent craze to produce integrative fuel typology and fuel metrics at the international level in Europe points in this direction (Aragoneses et al., 2024, Kurtchartt et al., 2024).

Fig. 7 illustrates relationships between our direct ALS-based estimation of fuel load and density (CFL and CBD) and allometric field-based estimates. Similar to CBH, relationships for profile type "A" between ALS and field-based fuel load metrics presented moderate to high goodness of fit ($R^2 = 0.42$ and 0.67 and nRMSE = 14 % and 23 % for CFL and CBD respectively) and low bias (nbias = −2 % et −3.3 % for CFL and CBD respectively). These results are similar to classical supervised classification approaches trained on field data in the literature with R^2 ranging from 0.30 to 0.70 for CBD in Mediterranean forests (Botequim et al., 2019; Crespo-Peremarch et al., 2016; Marino et al., 2022). Thus it is encouraging to observe such results with our direct ALS-based estimates of fuel load, which are completely independent of field data. It is also worth noting that the range of CFL and CBD estimates using our direct ALS-based approach agrees well with field data values for profile type "D" with a nbias of 12 % in spite of poor goodness of fit (0.09 and 0.14 for CFL and CBD respectively). This profile type groups 72 % of the plots (i.e. 292).

3.2.3. *Contribution of species-specific plant traits for fuel metrics estimates based on als*

The fine fuel estimates obtained with our ALS approach from PAD required a conversion factor from fuel area to fuel biomass. Plant traits allowing this conversion (i.e. LMA and WD for FMA calculation) are increasingly available at species level thanks to large worldwide databases (Díaz et al., 2022) and were used in the present study for deriving PAD profiles to bulk density profiles and estimating fuel load metrics (see Section 2.2.1.5). Table 4 illustrates statistics on the relationships between field-based and ALS-based fuel load metrics when species-specific plant traits were used ("Sp-PT" in Table 4) or not ("*Av*-PT" in Table 4: corresponding to average FMA value). Overall, the goodness of fit and bias were better when species-specific traits were considered. These results are particularly clear for plots having a FPT "A" but also regarding the statistics of all plots mixed together.

Fig. 8 illustrates the deviation between ALS-based and field-based CFL by species. Note that only species dominant in more than five plots and having a FMA at least 30 % higher or lower than the average FMA were kept for the analyses. CBD results are not presented here but were similar. A value of 0 in Fig. 8 means that the ALS-based CFL is equal to the field-based CFL estimates. The results highlight that ALS tended to

Table 4
Statistics of the relationship between ALS-based and field-based fuel load metrics (CFL and CBD) when using species-specific plants traits (Sp-PT) and average plant traits (*Av*-PT). See section 2.2.1.3.

	CFL						CBD						N
	R^2		nRMSE		nbias		R^2		nRMSE		nbias		
	***Av*-PT**	**Sp-PT**	***Av*-PT**	**SP-PT**	***Av*-PT**	**Sp-PT**	***Av*-PT**	**Sp-PT**	***Av*-PT**	**Sp-PT**	***Av*-PT**	**Sp-PT**	
FPT													
A	0.37	0.42	136	14	20	2	0.57	0.67	151	22	22	3	48
B	0.23	0.23	339	228	44	30	0.33	0.34	350	237	46	31	59
C	0.22	0.29	187	164	59	52	−0.06	−0.01	184	164	58	52	10
D	0.02	0.08	87	245	−5	−14	0.07	0.14	60	230	−4	−13	292
All													
A,B,C,D	0.09	0.18	236	1	12	0	0.16	0.28	239	6	12	0	409

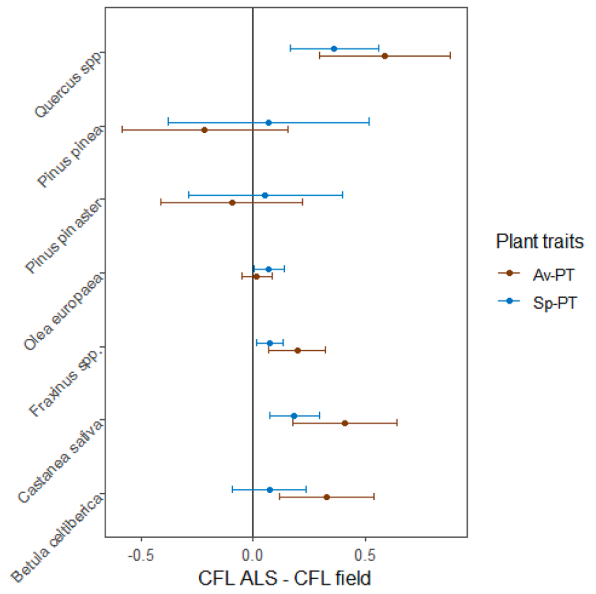

Fig. 8. Plant traits effect on differences between field-based and ALS-based CFL. Only species dominant in >5 plots are shown. Mean differences and standard deviation are respectively represented by dots and error bars. The closest the value to 0 the more consistent field and ALS-based CFL. In blue species-specific plant traits (Sp-PT) were used to estimate FMA in brown average plant traits (*Av*-PT) value was used. Field canopy strata boundaries are used (i.e. field CBH and field mean tree height) to compute ALS-based fuel metrics. Average FMA: 0.25 kg/m^2. Species-specific FMA: Quercus spp: 0.17; Pinus pinea: 0.39; Olea Europea: 0.34; Fraxinus spp: 0.14; Castanea sativa: 0.14; Betula celtiberica: 0.14.

underestimate CFL for coniferous species (when using average plant traits) while it overestimated it for broadleaved species. The canopy structure (i.e. shape and organization of leaves and twigs) of these two functional groups interact differently with LiDAR signals. The cylindrical shape of needle-leaved species and their twig insertion exposed a reduced proportion of the surface to laser beam compared to broadleaves resulting in potential underestimation of PAD and thus of bulk density. Interestingly, using species specific plant traits for converting plant area to fuel biomass (i.e."Sp-PT" in Table 4 and Fig. 8) tended to reduce the deviation between ALS and field-based fuel load estimates for six of the seven species analyzed (but significantly for three species only, the two *Pinus* and the *Quercus* spp.). These results highlight the importance of accurate vegetation type mapping. The traits of dominant canopy species were considered here only. A great step forward would be to adapt plant traits values to the height on the profile to consider understory species traits in the fuel metrics estimates.

Importantly, the inversion of the radiative transfer model used to obtain PAD from LiDAR point cloud hypothesizes homogeneous plant elements distribution when a clumping factor Ω of 1 is used in Eq. (4). This hypothesis is violated in the context of natural vegetation at our scale of analysis (i.e. 12.62-m radius plot, see Table 1) and a constant correction factor of the vegetation clumping was therefore used (i.e. Ω = 0.77, see Appendix 1). However, more research is needed to correctly integrate the clumping index according to vegetation type and structure and more specifically vegetation cover that is directly related to the clumping factor at those scales of analysis (Chen et al., 2005). Basically, integrating a vegetation-structure-dependent clumping factor might reduce the rest of the bias observed for certain species with high bias (Table 4 and Fig. 8). The next step forward will be an integrative approach with ALS data that uses the point cloud to estimate this clumping factor as already explored by Hu et al. (2018).

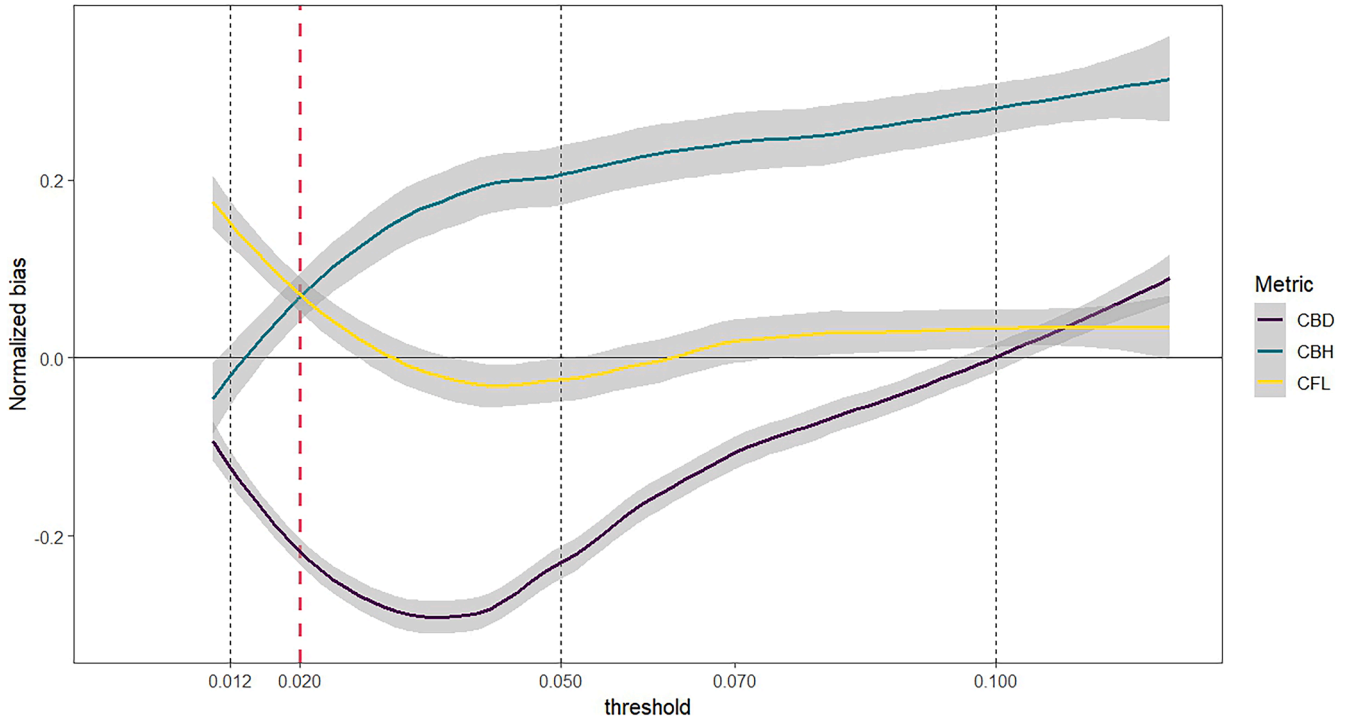

Fig. 9. Normalized bias of three key fuel metrics according to the bulk density threshold used to compute them. ALS-based metrics overestimate or underestimate the metrics (compared to field-based) when the bias is positive or negative respectively. The red dashed vertical line represents the bulk density threshold minimizing both CFL and CBH normalized bias. The black dashed vertical lines represent several key CBD values in terms of fire behavior modelling (Reinardt et al., 2006; Alexander and Cruz, 2013).

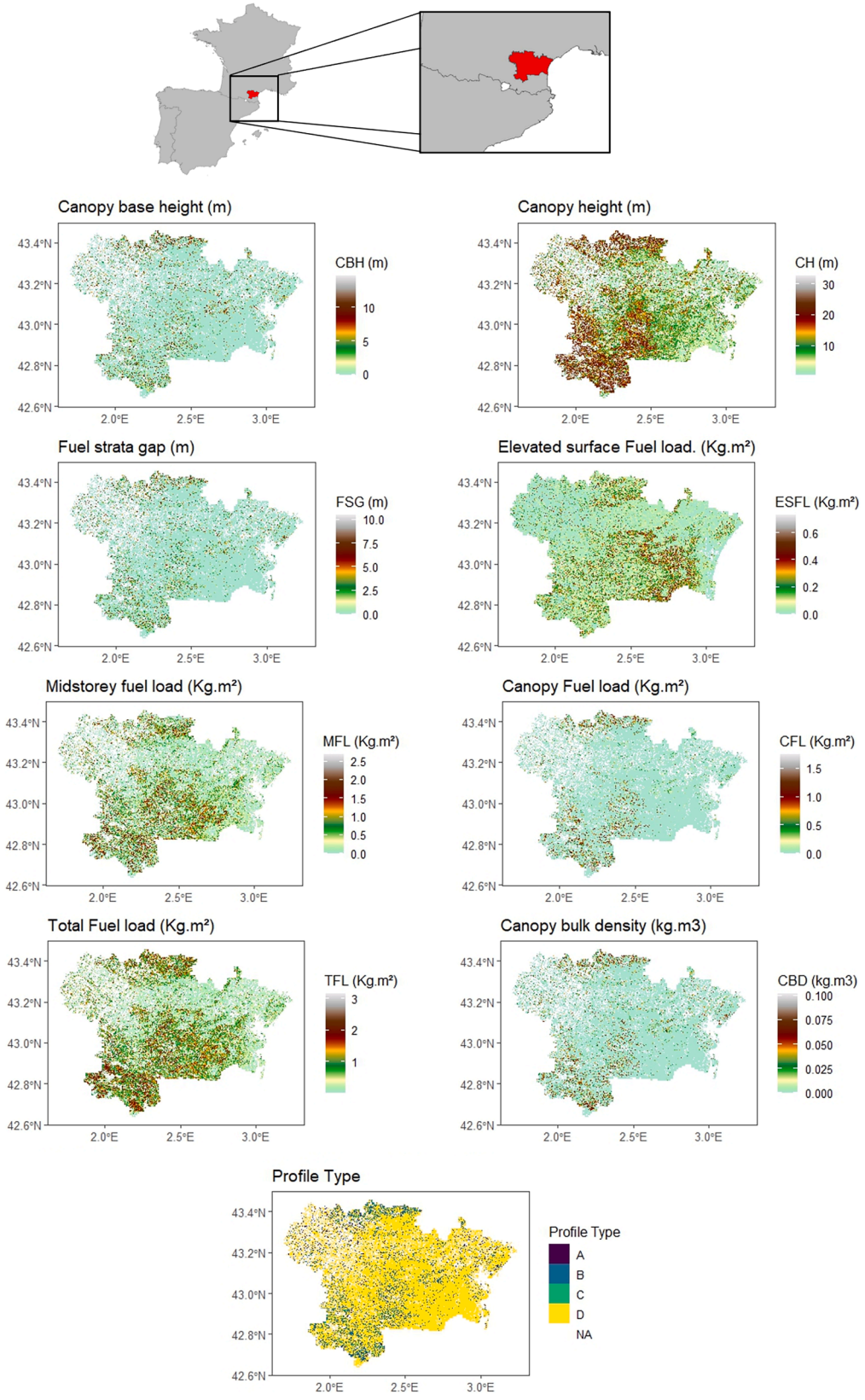

Fig. 10. Example of nine fuel metrics mapped at large scale derived from ALS data (Fig. 3 & Table 3). The mapped area is the French administrative unit of Aude (6343 km^2) in southern France dominated by Mediterranean vegetations. Metrics are derived from ALS-based bulk density profiles by using a threshold value of 0.02 kg/m3. Metrics are computed at 20m.

3.3. Absolute bulk density threshold identification for fuel metrics mapping

The previous sections results aimed at evaluating the potential of our ALS-based approach to retrieve fuel metrics obtained from field data and allometries. In this context we used field canopy boundaries (field CBH and stand height) to quantify CFL and CBD with our ALS-based approach. However, identifying CBH and its dependent fuel metrics (i.e. CFL, MFL, CBD, FSG, profile type) from bulk density profiles using ALS data only require defining a bulk density threshold. The question of selecting a reliable and integrative (or species dependent) bulk density threshold for estimating canopy fuel metrics remains and can only be achieved by experimental work and measurement or by theoretical physical modelling approaches and is out of the scope of this study. However, several thresholds to identify CBH were mentioned in the literature (Cruz and Alexander, 2010). A threshold of 0.012 kg m^{-3} was proposed by Reinhardt et al. (2001) and has been commonly used to determine CBH (Arkin et al., 2023) even though the authors acknowledged that arbitrarily defining such threshold can be criticized (Reinhardt et al., 2006). But if the model of Van Wagner (1977) is used to predict crown fire inception, then 0.05 kg m^{-3} should be adopted as the CBD threshold (Alexander and Cruz, 2014). Fig. 9 illustrates the normalized bias (using field estimates as reference) response of three metrics to a range of bulk density thresholds roughly matching the above-mentioned literature (i.e. from 0.01 to 0.1). 0.02 kg m^{-3} is the threshold minimizing CFL and CBH estimates and is used here to quantify CBH dependent metrics at the pixel scale for the mapping example (Fig. 10). However, this value is selected because it provides CBH and CFL estimates close to field and is therefore consistent for both forestry assessment of CBH and fuel load allometric estimation in the dataset we used, but is not related to any fire behavior consideration. A detailed sensitivity analysis of ALS-based fuel metrics to bulk density threshold is described in Appendix 3.

Fig. 10 illustrates an example of large-area fuel mapping from ALS-derived bulk density profiles in 20-m resolution pixels for a French NUTS3 region ("Aude" Departement, 6343 km^2). Beyond CBH, CBD, and CFL, this example shows how bulk density profiles can be easily used to map other relevant fuel metrics. As an example, FSG is hard to estimate on the field but is of great importance for modeling crown fire behavior (Cruz et al., 2004; Perrakis et al., 2023). Moreover, these profiles and our characterization of fire-physics oriented strata (elevated surface, midstory, gap strata and canopy strata) allowed mapping the fuel loads that would be consumed by fire (above a specified amount of fuel, i.e. bulk density threshold), depending on the type of fire (surface or crown fire), which is critical to estimate potential fireline intensity. Bulk density profiles also allow estimating fuel load in the elevated surface (0–1 m) and midstory strata that are directly involved in fire ignition and surface fire propagation. Note however that the ESFL has larger uncertainties compared to other strata as discussed in section 3.1 and is focused on standing fuel and therefore excludes coarse woody debris and litter. Moreover, profile shape typologies such as those proposed in this study (i.e. FPT: A,B,C,D) characterize qualitatively the continuity and complexity of fuel vertical organization. These profile types can be of great interest for creating new fuel typologies or precising already existing ones for assessing fire hazard and targeting forest management practices. Finally, it is interesting to note that in the Mediterranean a large proportion of the forest features a continuous fuel organization. As a result, 75.5 % of the pixels in the forested area mapped on Fig. 10 are characterized by a profile type "D" and therefore had no meaningful CBH values. Similarly, 74 % of the Spanish and Portuguese plots belonged to FPT "D". This highlights the importance of considering the vertical organization of vegetation as a whole and questions the relevance of using tree-based CBH for fire behavior modelling in such ecosystems.

4. Conclusion

We proposed in this paper a method to directly derive fuel metrics from ALS point cloud regardless vegetation type. This approach takes full advantages of ALS three-dimensional data to capture the bulk density vertical profile, is highly generalist because it takes into account sampling heterogeneities (i.e. variability in point cloud density), scanning pattern differences and occlusion and can therefore be applied irrespective of the LiDAR sensors devices, flying patterns or vegetation types. The derived vegetation profiles and fuel metrics were consistent with field data. Further research is needed to exploit more confidently the closest-to-ground strata (0–0.5 m). Integrating plot or pixel-dependent clumping factors for correcting fuel area estimates using the radiative transfer approach would be a next step forward for improving the method and will be explored in a following study.

Finally, the potential of our approach for mapping many useful quantitative fuel load and structural metrics based on vertical bulk density distribution was demonstrated. This approach fits well into the recent calls of the Canadian Forest service fire danger group (2021) for reengineering the fire behavior modelling approach by including more flexibility in stand structure description instead of adopting generic typologies. This approach should contribute to change the paradigm of "reference field data" at this scale of analysis and that precise LiDAR-based approaches such as the one proposed in this study could be used as reference data to train models based on high frequency and high-resolution remote sensing products.

Funding

This work was supported by the European Horizon 2020 research and Innovation Programme under grant agreement n° 101,037,419, through the project FIRE-RES–Innovative technologies and socio-economic solutions for fire-resistant territories in Europe. This research was supported by the grant funded by the Foundation for Science and Technology (FCT), Portugal to Guerra-Hernández (CEECIND/02,576/2022). The project LiDARCAT3, which covers Catalonia with LiDAR data, was funded through the European Next Generation funds as part of the Recovery, Transformation, and Resilience Plan, affiliated with the *Ministerio para la Transición Ecológica y el Reto Demográfico* (MITECO), and coordinated by the IGN (*Instituto Geográfico Nacional*). Fuel maps for the example Nuts3 "Aude" were developed for the ALEOFEU research project funded by the SCO grant of the National French Spatial Agency (CNES), with financial support of the Ministry of Ecology (MTECT). PMF was supported by National Funds from FCT - Portuguese Foundation for Science and Technology, under project UIDB/04,033/2020 (https://doi.org/10.54499/UIDB/04033/2020).

CRediT authorship contribution statement

Olivier Martin-Ducup: Writing – review & editing, Writing – original draft, Methodology, Investigation, Formal analysis, Data curation, Conceptualization. **Jean-Luc Dupuy:** Writing – review & editing, Supervision, Resources, Funding acquisition. **Maxime Soma:** Writing – review & editing, Data curation. **Juan Guerra-Hernandez:** Writing – review & editing, Data curation. **Eva Marino:** Writing – review & editing, Data curation. **Paulo M. Fernandes:** Writing – review & editing. **Ariadna Just:** Writing – review & editing, Data curation. **Jordi Corbera:** Writing – review & editing, Data curation. **Marion Toutchkov:** Writing – review & editing, Data curation. **Charlie Sorribas:** Writing – review & editing, Data curation. **Jerome Bock:** Writing – review & editing, Methodology. **Alexandre Piboule:** Writing – review & editing, Methodology, Investigation. **Francesco Pirotti:** Writing – review & editing. **François Pimont:** Writing – review & editing, Validation, Supervision, Resources, Methodology, Investigation, Conceptualization.

Declaration of competing interest

The authors declare the following financial interests/personal relationships which may be considered as potential competing interests:

Olivier Martin-Ducup reports financial support was provided by Horizon Europe. Juan Guerra-Hernandez reports financial support was provided by Foundation for Science and Technology. Ariadna Just reports financial support was provided by Spain Ministry for the Ecological Transition and Demographic Challenge. Francois Pimont reports financial support was provided by French Space Agency. If there are other authors, they declare that they have no known competing financial interests or personal relationships that could have appeared to influence the work reported in this paper.

Acknowledgments

The ForestWISE–Collaborative Laboratory for Integrated Forest and Fire Management is acknowledged for making available the ground data and the enhanced plot positioning information of the project áGiL. The fire department (DFCI) of the French national forest service (ONF) is acknowledged for collecting and sharing the vegetation cover data.

Supplementary materials

Supplementary material associated with this article can be found, in the online version, at doi:10.1016/j.agrformet.2024.110341.

Appendix 1: Determining a clumping index (Ω) value for inverting transmittance into plant area density (PAD)

The clumping index Ω is used in the light transmittance Eq. (2) and describes the aggregation of vegetation in the canopy volume. At our scale of analysis (~500m²) Ω likely varies between 0.5 (highly clumped vegetation element) to 1 (homogeneous vegetation elements) depending on vegetation type and cover (Chen et al., 2005). For identifying a constant Ω value for all the vegetation plots analyzed in the present study we selected the Ω that optimizes the canopy fuel load bias of the 410 vegetation plots.

$$Normalized\ CFL\ bias = \frac{\frac{1}{n}\sum_{i=1}^{n} CFL_{ALS_i} - CFL_{Field_i}}{mean\ (CFL_{ALS})}$$

In order to compare fuel load estimates in the same canopy volume the field canopy boundaries (field CBH and field mean tree height) were used for quantifying CFL_{ALS}.

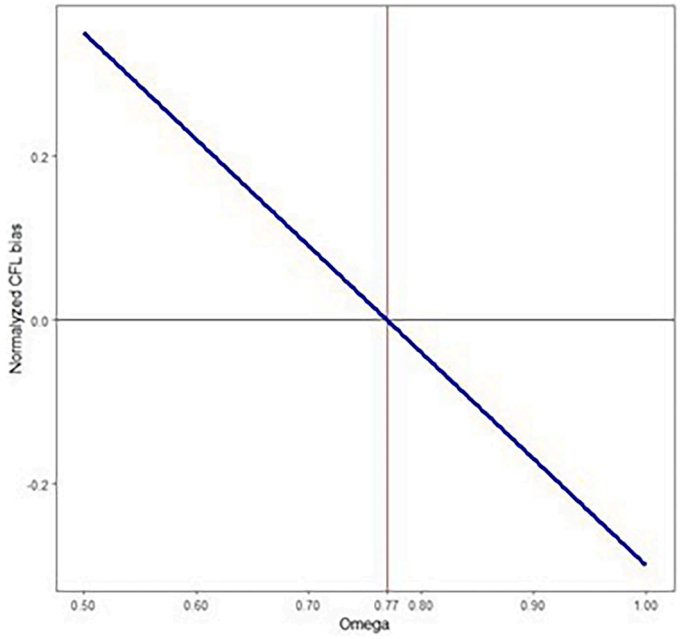

Fig. A1. Relationship between Ω parameter value and the normalized CFL bias. The vertical red line symbolizes the Ω value minimizing the normalized CFL bias (i.e. 0.77).

Fig. A1 illustrates the relationship between the normalized CFL bias and the Ω value varying between 0.5 and 1 (0.01 step). The optimal value in terms of bias (~0) is Ω=0.77 and is retained and remains constant for the rest of the study. It is interesting to note that the value that minimizes the bias fall in the whole range (minimum to maximum) of literature (Ω=0.55 to 0.85 for minimum and maximum value resp.), and that overall, the CFL bias never exceed 16 % in the range of vegetation type average literature values (Ω= 0.62 to 0.77) (cf Table 4 in Chen et al. 2005).

Further research is needed for obtaining an adaptative Ω value based on the point cloud. This would allow to reduce uncertainties due to vegetation structure on LAD estimates but is out of the scope of the present work. This subject will be explored further in an upcoming study.

Appendix 2: Real world bulk density profiles

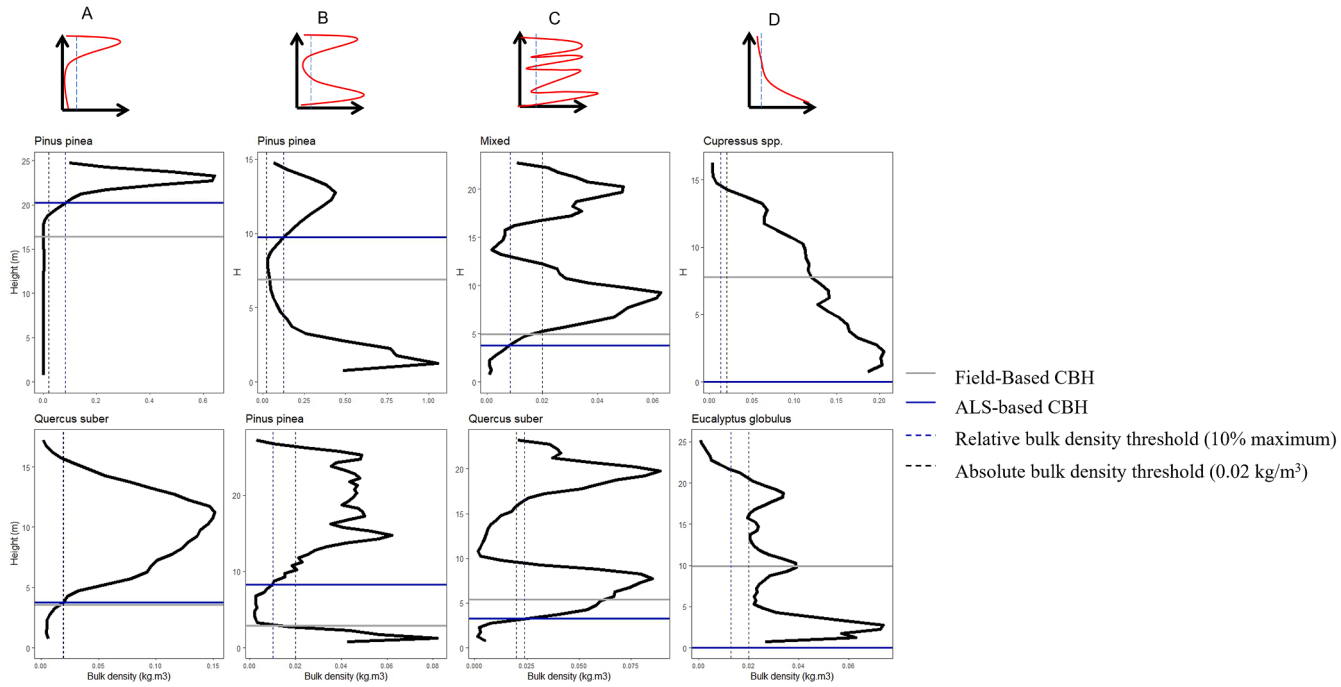

Fig. A2. Example of real-world bulk density profiles of the four FPT (i.e. A, B, C and D) extracted from LiDAR data and the corresponding field-based (grey horizontal line) and ALS-based (blue horizontal line) CBH for eight plots. The vertical dashed lines correspond to i) the relative (10 % of maximum bulk density) threshold used to estimates the CBH in blue and ii) the absolute threshold 0.02 kg/m^3 identified as the threshold minimizing the CFL bias.

Fig. A2 illustrates two different bulk density profiles for each of the four FPTs in practice. The plot profiles shown differ in terms of structure and composition (i.e. dominance of *Pinus pinea, Quercus suber, Cupressus spp* or *Eucalyptus globulus* or mixed stand). FPT "A" illustrates how both ALS-based and field-based CBH can be consistent in these simple plots for the *Quercus suber* plot example, but also how a difference > 4 m for CBH can be observed for *Pinus pinea* due to i) an underestimation in the field and ii) the subjective choice of a relative threshold for the *Pinus pinea* plot example. As expected, FPT "B" shows a clear bi-layered profile, even though the lower profile shows a more complex structure in the canopy stratum. In these examples, the ALS-based CBH appeared to better match the vertical structure of the plots. It is also interesting to note that using an absolute threshold of 0.02 kg/m^3 for the upper profile would result in a change of FPT from "B" to "D". FPT "C" represents a structure without continuous midstory strata but with two fuel strata gap and two vegetation strata. The methodological choice of using the first fuel strata gap to define the canopy stratum results in the ALS-based CBH being below the first stratum, but this is consistent with the field assessment of CBH in both cases (i.e. mixed and *Quercus suber* stands). In this context, note that the canopy layer is everything above the CBH (see definition of canopy strata in Table 3), including the upper FSG, even though there may not be enough fuel in the higher vegetation layer to spread fire. FPT "D" exhibits two different structures, "near linear" for *Cupressus* spp. and "complex" for *Eucalyptus globulus*, but neither exhibits a gap between fuel strata as dictated by the threshold used. These continuous profiles result in an ALS-based CBH of 0, although the structure could indicate the presence of one (or more) vegetation strata, as observed for the *Eucalyptus globulus* stand and highlighted by the identification of field-based CBH of 10 m in one of these strata.

Appendix 3: Sensitivity of ALS-based metrics to different bulk density threshold values

Method

CBH, FSG, MFL, CFL and CBD values were generated on each Portuguese plot for twenty different bulk density threshold values from 0.01 to 0.1 kg/m^3. The relative values of the metrics for a given threshold *i* ($rMetric_i$) were used (i.e., rCBH, rFSG, rCFL, rMFL, rCBD) so that the effects of bulk density thresholds are comparable between plots with very different metric values. For a given threshold *i* the relative metrics are calculated as follows:

$$rMetric_i = \frac{Metric_i}{max\left(Metric_{i1,i2,i3\ldots i20.}\right)} \quad (13)$$

with $Metric_i$ the value of a fuel metric in a plot for threshold *i.*

In order to visually observe the sensitivity of metrics to threshold value, the relationships between bulk density threshold value and $rMetric_i$ were fitted using general additive models (gam).

Results

Results are illustrated on Fig. A3. An overall positive trend is observed for CBH, with rCBH varying by a factor of two (i.e. 0.5 to 1) in the range of the bulk density threshold tested (i.e. 0.01 to 0.1) for all profile types but particularly evident for profile type "A" and "C", with larger fluctuation for

the latter (i.e. large confidence interval). The bi-layer profile type “B" presents a weaker response because CBH is identified either on the lower or on the upper strata depending on the threshold. The profile type “D" also showed a weaker trend likely due to the same reason. Very similar trends for all profile types are observed for rFSG (but varying by a factor of ~3), which was expected as CBH and CFL are closely related. rCFL overall decrease for all FPT due to a shortening in canopy volume because of increasing CBH. The trend is particularly clear for simple FPT (i.e. “A”) and absent for profile type B likely due to the same behavior of CBH identified in the lower of upper strata depending on threshold values. An overall inverse trend is observed for rCBD because as CBH increases the canopy volume decreases leading to high fuel load density. rCFL and rCBD presents overall less sensitivity than rCBH and rFSG and vary by a factor of ~1.5. rMFL decrease as the threshold increases because of a reduction of the midstory volume for all FPT except “C". A very steep decrease to rMFL = 0 is observed for FPT “A" corresponding to profiles without understory at 10 % maximum bulk density threshold. This indicates that almost all FPT “A" do not have midstory strata when a threshold value of ~ 0.03 kg/m^3 is considered.

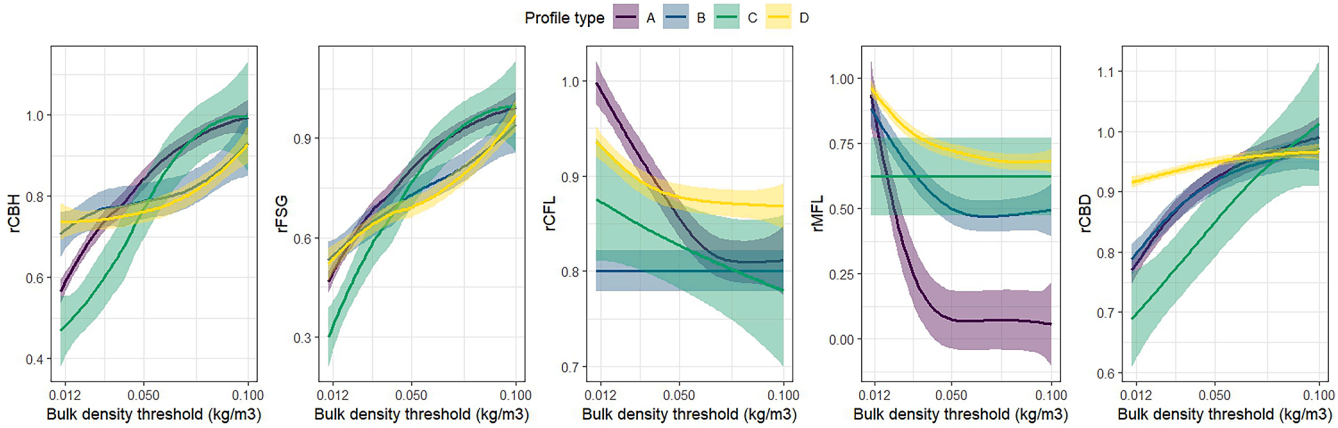

Fig. A3. Sensitivity of five fuel metrics to the bulk density threshold used (from 0.01 to 0.1). The lines represent a generalized additive model (Gam) smoothing function and the shaded area is the 95 % confidence interval. For each plot, the relative values of the metrics are used (i.e., rCBH, rFSG, rCFL, rCBD, rCMFL) so that the effects of threshold are comparable between plots with different metric values. Each profile type (Fig. 3) based on a 10 % bulk density threshold is shown separately (color scale).

Data availability

The package LidarForFuel developed in the context of this study is available on the github repository: https://github.com/oliviermartin7/LidarForFuel. DOI: 10.5281/zenodo.14261023.

References

Abdollahi, A., Yebra, M., 2023. Forest fuel type classification: review of remote sensing techniques, constraints and future trends. J. Environ. Manage. 342, 118315. https://doi.org/10.1016/j.jenvman.2023.118315.

Alexander, M.E., Cruz, M.G., 2013. Limitations on the accuracy of model predictions of wildland fire behaviour: a state-of-the-knowledge overview. Forest. Chron. 89, 372–383. https://doi.org/10.5558/tfc2013-067.

Alexander, M.E., Cruz, M.G., 2014. Tables for Estimating Canopy Fuel Characteristics from Stand Variables in Four Interior West Conifer Forest Types. Forest Sci. 60, 784–794. https://doi.org/10.5849/forsci.13-506.

Aragoneses, E., García, M., Salis, M., Ribeiro, L.M., Chuvieco, E., 2023. Classification and mapping of European fuels using a hierarchical, multipurpose fuel classification system. Earth Syst. Sci. Data 15, 1287–1315. https://doi.org/10.5194/essd-15-1287-2023.

Aragoneses, E., García, M., Ruiz-Benito, P., Chuvieco, E., 2024. Mapping forest canopy fuel parameters at European scale using spaceborne LiDAR and satellite data. Remote Sens Environ 303, 114005. https://doi.org/10.1016/j.rse.2024.114005.

Arkin, J., Coops, N.C., Daniels, L.D., Plowright, A., 2023. Canopy and surface fuel estimations using RPAS and ground-based point clouds. Forestry. https://doi.org/10.1093/forestry/cpad020 cpad020.

Armand, D., Etienne, M., Legrand, C., Marechal, J., Valette, J.C., 1993. Phytovolume, phytomasse et relations structurales chez quelques arbustes méditerranéens. Ann. For. Sci. 50, 79–89. https://doi.org/10.1051/forest:19930106.

Arroyo, L.A., Pascual, C., Manzanera, J.A., 2008. Fire models and methods to map fuel types: the role of remote sensing. For. Ecol. Manage. 256, 1239–1252. https://doi.org/10.1016/j.foreco.2008.06.048.

Béland, M., Widlowski, J.L., Fournier, R.A., Côté, J.F., Verstraete, M.M., 2011. Estimating leaf area distribution in savanna trees from terrestrial LiDAR measurements. Agric. For. Meteorol. 151, 1252–1266.

Béland, M., Widlowski, J.-L., Fournier, R.A., 2014. A model for deriving voxel-level tree leaf area density estimates from ground-based LiDAR. Environ. Modell. Softw. 51, 184–189. https://doi.org/10.1016/j.envsoft.2013.09.034.

Botequim, B., Fernandes, P.M., Borges, J.G., González-Ferreiro, E., Guerra-Hernández, J., 2019. Improving silvicultural practices for Mediterranean forests through fire behaviour modelling using LiDAR-derived canopy fuel characteristics. Int. J. Wildland Fire 28, 823–839. https://doi.org/10.1071/WF19001.

Bouvier, M., Durrieu, S., Fournier, R.A., Renaud, J.-P., 2015. Generalizing predictive models of forest inventory attributes using an area-based approach with airborne LiDAR data. Remote Sens. Environ 156, 322–334. https://doi.org/10.1016/j.rse.2014.10.004.

Bright, B.C., Hudak, A.T., Meddens, A.J.H., Hawbaker, T.J., Briggs, J.S., Kennedy, R.E., 2017. Prediction of forest canopy and surface fuels from Lidar and satellite time series data in a bark beetle-affected forest. Forests 8, 322. https://doi.org/10.3390/f8090322.

Byram, G.M., 1959. Combustion of forest fuels. ‘Forest fire: Control and Use. KP Davis, pp. 61–89.

Cameron, H.A., Díaz, G.M., Beverly, J.L., 2021. Estimating canopy fuel load with hemispherical photographs: a rapid method for opportunistic fuel documentation with smartphones. Methods Ecol. Evol. 12, 2101–2108. https://doi.org/10.1111/2041-210X.13708.

Campbell, M.J., Dennison, P.E., Hudak, A.T., Parham, L.M., Butler, B.W., 2018. Quantifying understory vegetation density using small-footprint airborne lidar. Remote Sens. Environ 215, 330–342. https://doi.org/10.1016/j.rse.2018.06.023.

Canadian Forest Service Fire Danger Group. 2021. An overview of the next generation of the Canadian Forest Fire Danger Rating System. (Information Report GLC-X-26). Natural Resources Canada, Canadian Forest Service, Great Lakes Forestry Centre. Information Report GLC-X-26. 70 p.

Chamberlain, C.P., Sánchez Meador, A.J., Thode, A.E., 2021. Airborne lidar provides reliable estimates of canopy base height and canopy bulk density in southwestern ponderosa pine forests. For. Ecol. Manage. 481, 118695. https://doi.org/10.1016/j.foreco.2020.118695.

Chave, J., Coomes, D., Jansen, S., Lewis, S.L., Swenson, N.G., Zanne, A.E., 2009. Towards a worldwide wood economics spectrum. Ecol. Lett. 12, 351–366. https://doi.org/10.1111/j.1461-0248.2009.01285.x.

Chen, J.M., Menges, C.H., Leblanc, S.G., 2005. Global mapping of foliage clumping index using multi-angular satellite data. Remote Sens. Environ 97, 447–457. https://doi.org/10.1016/j.rse.2005.05.003.

Choat, B., Jansen, S., Brodribb, T.J., Cochard, H., Delzon, S., Bhaskar, R., Bucci, S.J., Feild, T.S., Gleason, S.M., Hacke, U.G., Jacobsen, A.L., Lens, F., Maherali, H., Martínez-Vilalta, J., Mayr, S., Mencuccini, M., Mitchell, P.J., Nardini, A., Pittermann, J., Pratt, R.B., Sperry, J.S., Westoby, M., Wright, I.J., Zanne, A.E., 2012. Global convergence in the vulnerability of forests to drought. Nature 491, 752–755. https://doi.org/10.1038/nature11688.

Clark, J., Murphy, G., 2011. Estimating forest biomass components with hemispherical photography for Douglas-fir stands in northwest Oregon. Can. J. For. Res. 41, 1060–1074. https://doi.org/10.1139/x11-013.

Crespo-Peremarch, P., Ruiz, L.A., Balaguer-Beser, Á., 2016. A comparative study of regression methods to predict forest structure and canopy fuel variables from LiDAR

full-waveform data. Revista de Teledetección 27–40. https://doi.org/10.4995/raet.2016.4066.
Cruz, M.G., Alexander, M.E., 2010. Assessing crown fire potential in coniferous forests of western North America: a critique of current approaches and recent simulation studies. Int. J. Wildland Fire 19, 377–398. https://doi.org/10.1071/WF08132.
Cruz, M.G., Alexander, M.E., 2013. Uncertainty associated with model predictions of surface and crown fire rates of spread. Environ. Modell. Softw. 47, 16–28. https://doi.org/10.1016/j.envsoft.2013.04.004.
Cruz, M.G., Alexander, M.E., Wakimoto, R.H., 2003. Assessing canopy fuel stratum characteristics in crown fire prone fuel types of western North America. Int. J. Wildland Fire 12, 39–50. https://doi.org/10.1071/wf02024.
Cruz, M.G., Alexander, M.E., Wakimoto, R.H., 2004. Modeling the likelihood of crown fire occurrence in conifer forest stands. Forest Sci. 50, 640–658. https://doi.org/10.1093/forestscience/50.5.640.
Cruz, M.G., Butler, B.W., Alexander, M.E., Forthofer, J.M., Wakimoto, R.H., Cruz, M.G., Butler, B.W., Alexander, M.E., Forthofer, J.M., Wakimoto, R.H., 2006. Predicting the ignition of crown fuels above a spreading surface fire. Part I: model idealization. Int. J. Wildland Fire 15, 47–60. https://doi.org/10.1071/WF04061.
Díaz, S., Kattge, J., Cornelissen, J.H.C., Wright, I.J., Lavorel, S., Dray, S., Reu, B., Kleyer, M., Wirth, C., Prentice, I.C., Garnier, E., Bönisch, G., Westoby, M., Poorter, H., Reich, P.B., Moles, A.T., Dickie, J., Zanne, A.E., Chave, J., Wright, S.J., Sheremetiev, S.N., Jactel, H., Baraloto, C., Cerabolini, B.E.L., Pierce, S., Shipley, B., Casanoves, F., Joswig, J.S., Günther, A., Falczuk, V., Rüger, N., Mahecha, M.D., Gorné, L.D., Amiaud, B., Atkin, O.K., Bahn, M., Baldocchi, D., Beckmann, M., Blonder, B., Bond, W., Bond-Lamberty, B., Brown, K., Burrascano, S., Byun, C., Campetella, G., Cavender-Bares, J., Chapin, F.S., Choat, B., Coomes, D.A., Cornwell, W.K., Craine, J., Craven, D., Dainese, M., de Araujo, A.C., de Vries, F.T., Domingues, T.F., Enquist, B.J., Fagúndez, J., Fang, J., Fernández-Méndez, F., Fernandez-Piedade, M.T., Ford, H., Forey, E., Freschet, G.T., Gachet, S., Gallagher, R., Green, W., Guerin, G.R., Gutiérrez, A.G., Harrison, S.P., Hattingh, W. N., He, T., Hickler, T., Higgins, S.I., Higuchi, P., Ilic, J., Jackson, R.B., Jalili, A., Jansen, S., Koike, F., König, C., Kraft, N., Kramer, K., Kreft, H., Kühn, I., Kurokawa, H., Lamb, E.G., Laughlin, D.C., Leishman, M., Lewis, S., Louault, F., Malhado, A.C.M., Manning, P., Meir, P., Mencuccini, M., Messier, J., Miller, R., Minden, V., Molofsky, J., Montgomery, R., Montserrat-Martí, G., Moretti, M., Müller, S., Niinemets, Ü., Ogaya, R., Öllerer, K., Onipchenko, V., Onoda, Y., Ozinga, W.A., Pausas, J.G., Peco, B., Penuelas, J., Pillar, V.D., Pladevall, C., Römermann, C., Sack, L., Salinas, N., Sandel, B., Sardans, J., Schamp, B., Scherer-Lorenzen, M., Schulze, E.-D., Schweingruber, F., Shiodera, S., Sosinski, Ê., Soudzilovskaia, N., Spasojevic, M.J., Swaine, E., Swenson, N., Tautenhahn, S., Thompson, K., Totte, A., Urrutia-Jalabert, R., Valladares, F., van Bodegom, P., Vasseur, F., Verheyen, K., Vile, D., Violle, C., von Holle, B., Weigelt, P., Weiher, E., Wiemann, M.C., Williams, M., Wright, J., Zotz, G., 2022. The global spectrum of plant form and function: enhanced species-level trait dataset. Sci Data 9, 755. https://doi.org/10.1038/s41597-022-01774-9.
De Cáceres, M., Casals, P., Gabriel, E., Castro, X., 2019. Scaling-up individual-level allometric equations to predict stand-level fuel loading in Mediterranean shrublands. Ann. For. Sci. 76, 1–17. https://doi.org/10.1007/s13595-019-0873-4.
Dupuy, J.-L., Morvan, D., 2005. Numerical study of a crown fire spreading toward a fuel break using a multiphase physical model. Int. J. Wildland Fire 14, 141–151. https://doi.org/10.1071/WF04028.
Fernández-Alonso, J.M., Alberdi, I., Álvarez-González, J.G., Vega, J.A., Cañellas, I., Ruiz-González, A.D., 2013. Canopy fuel characteristics in relation to crown fire potential in pine stands: analysis, modelling and classification. Eur. J. Forest Res 132, 363–377. https://doi.org/10.1007/s10342-012-0680-z.
Fernandes, P.M., 2009. Combining forest structure data and fuel modelling to classify fire hazard in Portugal. Ann. For. Sci. 66, 1–9.
Finney, M.A., 1998. FARSITE, Fire Area Simulator–model Development and Evaluation. U.S. Department of Agriculture, Forest Service, Rocky Mountain Research Station.
Forbes, B., Reilly, S., Clark, M., Ferrell, R., Kelly, A., Krause, P., Matley, C., O'Neil, M., Villasenor, M., Disney, M., Wilkes, P., Bentley, L.P., 2022. Comparing remote sensing and field-based approaches to estimate ladder fuels and predict wildfire burn severity. Front. For. Global Change 5.
Gómez-Vázquez, I., Crecente-Campo, F., Diéguez-Aranda, U., Castedo-Dorado, F., 2013. Modelling canopy fuel variables in Pinus pinaster Ait. and Pinus radiata D. Don stands in northwestern Spain. Ann. For. Sci. 70, 161–172. https://doi.org/10.1007/s13595-012-0245-9.
Gale, M.G., Cary, G.J., Van Dijk, A.I.J.M., Yebra, M., 2021. Forest fire fuel through the lens of remote sensing: review of approaches, challenges and future directions in the remote sensing of biotic determinants of fire behaviour. Remote Sens. Environ. 255, 112282. https://doi.org/10.1016/j.rse.2020.112282.
García, M., Danson, F.M., Riaño, D., Chuvieco, E., Ramirez, F.A., Bandugula, V., 2011. Terrestrial laser scanning to estimate plot-level forest canopy fuel properties. Int. J. Appl. Earth Observ. Geoinform. 13, 636–645. https://doi.org/10.1016/j.jag.2011.03.006.
González-Ferreiro, E., Arellano-Pérez, S., Castedo-Dorado, F., Hevia, A., Vega, J.A., Vega-Nieva, D., Álvarez-González, J.G., Ruiz-González, A.D., 2017. Modelling the vertical distribution of canopy fuel load using national forest inventory and low-density airbone laser scanning data. PLOS ONE 12, e0176114. https://doi.org/10.1371/journal.pone.0176114.
Hu, R., Yan, G., Nerry, F., Liu, Y., Jiang, Y., Wang, S., Chen, Y., Mu, X., Zhang, W., Xie, D., 2018. Using airborne laser scanner and path length distribution model to quantify clumping effect and estimate leaf area index. IEEE Transac. Geosci. Remote Sens. 56, 3196–3209. https://doi.org/10.1109/TGRS.2018.2794504.
Jakubowksi, M.K., Guo, Q., Collins, B., Stephens, S., Kelly, M., 2013. Predicting surface fuel models and fuel metrics using Lidar and CIR imagery in a dense, mountainous forest. Photogram. Eng. Remote Sens. 79, 37–49. https://doi.org/10.14358/PERS.79.1.37.
Just Orriols, A., Vayreda Duran, J., 2022. Segunda Edición De Los Mapas de Variables Biofísicas Del Arbolado de Cataluña. 8° Congreso Forestal Español.
Kane, V.R., Lutz, J.A., Roberts, S.L., Smith, D.F., McGaughey, R.J., Povak, N.A., Brooks, M.L., 2013. Landscape-scale effects of fire severity on mixed-conifer and red fir forest structure in Yosemite National Park. For. Ecol. Manage. 287, 17–31. https://doi.org/10.1016/j.foreco.2012.08.044.
Keane, R.E., Reinhardt, E.D., Scott, J., Gray, K., Reardon, J., 2005. Estimating forest canopy bulk density using six indirect methods. Can. J. For. Res. 35, 724–739. https://doi.org/10.1139/x04-213.
Keane, R.E., 2015. Wildland Fuel Fundamentals and Applications. Springer International Publishing, Cham. https://doi.org/10.1007/978-3-319-09015-3.
Kramer, H.A., Collins, B.M., Kelly, M., Stephens, S.L., 2014. Quantifying ladder fuels: a new approach using LiDAR. Forests 5, 1432–1453. https://doi.org/10.3390/f5061432.
Kurtchartt, E., González-Olabarria, J.R., Trasobares, A., Aquilué, N., Guerra-Hernández, J., Leónia, N., Sequeira, A.C., Brigite, B., Marius, H., Palaiologou, P., Cardil, A., Rogai, M., Vassilev, V., Pimont, F., Martin-Ducup, O., Pirotti, F., 2024. Satellite-based mapping of canopy fuels at the pan-European scale. Accepted in Geo-pastial information science.
Labenski, P., Ewald, M., Schmidtlein, S., Heinsch, F.A., Fassnacht, F.E., 2023. Quantifying surface fuels for fire modelling in temperate forests using airborne lidar and Sentinel-2: potential and limitations. Remote Sens. Environ 295, 113711. https://doi.org/10.1016/j.rse.2023.113711.
LiDAR H.D. | Géoservices [WWW Document], 2024. URL https://geoservices.ign.fr/lidarhd#telechargementclassifiees (accessed 10.22.24).
Lin, Y., West, G., 2016. Retrieval of effective leaf area index (LAIe) and leaf area density (LAD) profile at individual tree level using high density multi-return airborne LiDAR. Int. J. Appl. Earth Observ. Geoinform. 50, 150–158. https://doi.org/10.1016/j.jag.2016.03.014.
Lines, E.R., Zavala, M.A., Purves, D.W., Coomes, D.A., 2012. Predictable changes in aboveground allometry of trees along gradients of temperature, aridity and competition. Global Ecol. Biogeogr. 21, 1017–1028.
Marino, E., Ranz, P., Tomé, J.L., Noriega, M.Á., Esteban, J., Madrigal, J., 2016. Generation of high-resolution fuel model maps from discrete airborne laser scanner and Landsat-8 OLI: a low-cost and highly updated methodology for large areas. Remote Sens. Environ 187, 267–280. https://doi.org/10.1016/j.rse.2016.10.020.
Marino, E., Montes, F., Tomé, J.L., Navarro, J.A., Hernando, C., 2018. Vertical forest structure analysis for wildfire prevention: comparing airborne laser scanning data and stereoscopic hemispherical images. Int. J. Appl. Earth Obser. Geoinfor. 73, 438–449. https://doi.org/10.1016/j.jag.2018.07.015.
Marino, E., Tomé, J.L., Hernando, C., Guijarro, M., Madrigal, J., 2022. Transferability of airborne LiDAR data for canopy fuel mapping: effect of pulse density and model formulation. Fire 5, 126. https://doi.org/10.3390/fire5050126.
Mihajlovski, B., Fernandes, P.M., Pereira, J.M.C., Guerra-Hernández, J., 2023. Comparing Forest Understory Fuel Classification in Portugal Using Discrete Airborne Laser Scanning Data and Satellite Multi-Source Remote Sensing Data. Fire 6, 327. https://doi.org/10.3390/fire6090327.
Monsi, M., Saeki, T., 2005. On the factor light in plant communities and its importance for matter production. Ann. Bot. 95, 549–567. https://doi.org/10.1093/aob/mci052.
Nguyen, V.-T., Fournier, R.A., Côté, J.-F., Pimont, F., 2022. Estimation of vertical plant area density from single return terrestrial laser scanning point clouds acquired in forest environments. Remote Sens. Environ 279, 113115. https://doi.org/10.1016/j.rse.2022.113115.
Perrakis, D.D.B., Cruz, M.G., Alexander, M.E., Hanes, C.C., Thompson, D.K., Taylor, S.W., Stocks, B.J., 2023. Improved logistic models of crown fire probability in Canadian conifer forests. Int. J. Wildland Fire 32, 1455–1473. https://doi.org/10.1071/WF23074.
Pimont, F., Dupuy, J.-L., Rigolot, E., Prat, V., Piboule, A., 2015. Estimating leaf bulk density distribution in a tree canopy using terrestrial LiDAR and a straightforward calibration procedure. Remote Sens (Basel) 7, 7995–8018. https://doi.org/10.3390/rs70607995.
Pimont, F., Allard, D., Soma, M., Dupuy, J.-L., 2018. Estimators and confidence intervals for plant area density at voxel scale with T-LiDAR. Remote Sens Environ 215, 343–370. https://doi.org/10.1016/j.rse.2018.06.024.
Reinhardt, E., Scott, J., Gray, K., Keane, R., 2006. Estimating canopy fuel characteristics in five conifer stands in the western United States using tree and stand measurements. Can. J. For. Res. 36, 2803–2814. https://doi.org/10.1139/x06-157.
Ross, J., 1981. The Radiation Regime and Architecture of Plant Stands. Task for Vegetation Sciences 3. Springer, The Hague, The Netherlands, p. 391.
Rothermel, R.C., 1972. A mathematical model for predicting fire spread in wildland fuels. Intermountain Forest & Range Experiment Station. Department of Agriculture, Forest Service, U.S.
Roussel, J.-R., Auty, D., Coops, N.C., Tompalski, P., Goodbody, T.R.H., Meador, A.S., Bourdon, J.-F., de Boissieu, F., Achim, A., 2020a. lidR: an R package for analysis of airborne laser scanning (ALS) data. Remote Sens. Environ 251, 112061. https://doi.org/10.1016/j.rse.2020.112061.
Roussel, J.-R., Bourdon, J.-F., Achim, A., 2020b. Range-based intensity normalization of ALS data over forested areas using a sensor tracking method from multiple returns.
Sando, R.W., Wick, C.H., 1972. A Method of Evaluating Crown Fuels in Forest stands. Research Paper NC-84. U.S. Dept. of Agriculture, Forest Service, North Central Forest Experiment Station, St. Paul, MN, p. 84.

Scott, J.H., Reinhardt, E.D., 2001. Assessing Crown Fire Potential by Linking Models of Surface and Crown Fire Behavior. U.S. Department of Agriculture, Forest Service, Rocky Mountain Research Station.

Shaiek, O., Loustau, D., Trichet, P., Meredieu, C., Bachtobji, B., Garchi, S., EL Aouni, M. H., 2011. Generalized biomass equations for the main aboveground biomass components of maritime pine across contrasting environments. Ann. For. Sci. 68, 443–452. https://doi.org/10.1007/s13595-011-0044-8.

Soma, M., 2019. Estimation De La Distribution Spatiale De Surface Et De Biomasse Foliaires De Couverts Forestiers Méditerranéens à Partir De Nuages De Points Acquis Par Un LIDAR Terrestre (PhD Thesis). Aix-Marseille.

Tomé, M., Barreiro, S., Paulo, J.A., Faias, S.P., 2007. Seleção de equações para estimação de variáveis da árvore em inventários florestais a realizar em Portugal.

Van Wagner, C.E.V., 1977. Conditions for the start and spread of crown fire. Can. J. For. Res. 7, 23–34. https://doi.org/10.1139/x77-004.

Wallace, L., Hillman, S., Hally, B., Taneja, R., White, A., McGlade, J., 2022. Terrestrial laser scanning: an operational tool for fuel hazard mapping? Fire 5, 85. https://doi.org/10.3390/fire5040085.

Werth, P.A., Potter, B.E., Alexander, M.E., Clements, C.B., Cruz, M.G., Finney, M.A., Forthofer, J.M., Goodrick, S.L., Hoffman, C., Jolly, W.M., 2016. Synthesis of knowledge of extreme fire behavior: volume 2 for fire behavior specialists, researchers, and meteorologists. Gen. Tech. Rep. PNW-GTR-891. Portland, OR: US Department of Agriculture, Forest Service, Pacific Northwest Research Station. 258 p.

Wilson, N., Bradstock, R., Bedward, M., 2021. Detecting the effects of logging and wildfire on forest fuel structure using terrestrial laser scanning (TLS). For. Ecol. Manage. 488, 119037. https://doi.org/10.1016/j.foreco.2021.119037.